The apoplastic space of two wheat genotypes provide highly different environment for pathogen colonization: Insights from proteome and microbiome profiling

Carolina Sardinha Francisco[1,2], Mohammad Abukhalaf[3], Clara Igelmann[1], Johanna Gustke[1], Michael Habig[1], Liam Cassidy[3], Andreas Tholey[3], Eva Holtgrewe Stukenbrock[1,2]

[1] Environmental Genomics, Kiel University, Kiel, Germany

[2] Max Planck Institute for Evolutionary Biology, Plön, Germany

[3] Systematic Proteomics and Bioanalytic, Kiel University, Kiel, Germany

Corresponding author: estukenbrock@bot.uni-kiel.de and csardinha@bot.uni-kiel.de

ABSTRACT

The intercellular space comprising the plant apoplast harbors a diverse range of microorganisms. The apoplastic interface represents the main compartment for interactions between proteins produced and secreted by the plant and the microbial endophytes. The outcomes of these interactions can play a role in plant cell wall metabolism, stress tolerance, and plant-pathogen resistance. So far the underlying factors that determine microbiota composition in the apoplast are not fully understood. However, it is considered that cell wall composition, nutrient availability, and the plant immune system are main determinants of microbiota composition. The plant immune system is considered to play a crucial role in modulating microbiota composition through the recognition of specific microbe-associated molecular patterns and the activation of defense responses. Hereby the plant may restrict non-beneficial microbial members and facilitate the propagation of beneficial ones. In this study, we investigated changes in the apoplastic environment during pathogen invasion using wheat as a model system. Infection of wheat with Zymoseptoria tritici, a fungal pathogen, resulted in notable alterations in the apoplast composition, reduced microbial diversity, and the accumulation of antimicrobial defense metabolites. Intriguingly, certain core microbial members persisted even in the presence of pathogen-induced immune responses, indicating their ability to evade or tolerate host immune defenses. To further explore these dynamics, we developed a protocol for extracting apoplastic fluids from wheat leaves and conducted proteome analyses to characterize the dynamic environment of the wheat leaves. Our findings uncovered a highly variable apoplastic environment that selects for microbes with specific adaptations. Notably, a core microbial community enriched in the resistant wheat cultivar exhibited antagonistic activity against Z. tritici, suggesting a potential role in

conferring pathogen defense. This study advances our understanding of the dynamic interactions and adaptations of the wheat apoplastic microbiota during pathogen invasion, emphasizing the pivotal role of microbial interactions in pathogen defenses.

Introduction

Plants are hosts to complex communities of microorganisms that function together in symbiotic relationships that define the “plant metaorganism” (1, 2). Detailed studies of microbial communities in below and above ground tissues have demonstrated that different plant compartments host distinct microbial communities (reviewed in (3)). A large diversity of microorganisms colonizes the surface of plant tissues, while some microorganisms have adapted to colonize the interior of plant tissues. Hereby, also the apoplastic compartment, which is the intercellular space within plant tissues, hosts a diverse range of microorganisms, including both bacteria and fungi. The composition of the apoplastic microbiota can vary depending on the tissue type and the developmental stage of the plant, but it is considered to play a role in plant cell wall metabolism and stress tolerance, including pathogen resistance (4, 5).

As distinct plant compartments represent very different environments for microbial propagation, they may select for microbes with particular adaptations. In the apoplastic compartment, factors which may select for particular microbial partners include cell wall composition, nutrient availability and the host immune system. For example, experimental studies using mutants of *Arabidopsis* affected in cuticle synthesis showed a pronounced influence on microbiota composition (6). Moreover, the apoplast is generally a nutrient-poor environment, and therefore favors microorganisms that can utilize complex plant compounds and effectively scavenge nutrients (7). Importantly, the apoplast is the main compartment for interactions between proteins produced and secreted by the plant and the microbial endophytes. How these factors jointly shape the plant microbiota during the lifetime of a plant remains poorly understood. Yet, understanding how the apoplastic environment

101 shapes microbial diversity is crucial to our understanding of plants as metaorganisms
102 as well as to the development of synthetic microbial communities intended to
103 strengthen plant health in production systems.
104
105 Genetic and experimental studies of plant-microbiota interactions have demonstrated
106 a fundamental role of the plant immune system in shaping microbiota composition. For
107 example, mutants of *A. thaliana* impaired in different immune-related signaling
108 pathways showed altered composition of their microbiota (e.g., (8, 9). Likewise,
109 activation of systemic immune responses in wheat, *Triticum aestivum*, by an avirulent
110 pathogen, conferred a significant shift in microbiota composition correlating with the
111 production of defense related metabolites (10). The evident function of the plant
112 immune system in shaping microbiota composition leads to the general assumption
113 that plants, via immune signaling, can regulate microbiota composition by selecting for
114 beneficial microbial partners and eliminating non-beneficial, pathogenic microbes.
115 Conceptually, these different types of microbial regulations have been termed
116 “recognition and tolerance" and "recognition and defense" responses (3, 11). At the
117 core of these interactions are pattern recognition receptors (PRR proteins) which are
118 embedded in plant membranes and act to recognize and distinguish particular microbe
119 associated molecular patterns (MAMPs) produced by microorganisms (12, 13). The
120 activation of defense signaling involves the production of reactive oxygen species
121 (ROS) and specific antimicrobial metabolites, modification of cell wall compositions,
122 and eventually local cell death. Such "recognition and defense responses” may lead
123 to the elimination of certain microorganisms, while simultaneously selecting for other
124 microorganisms that can tolerate a higher abundance of plant defense compounds
125 (9). This scenario invokes that core members of the plant metaorganism have adapted

126 to tolerate defense-related plant compounds, which are recurrently induced by
127 invading non-beneficial and pathogenic microorganisms.
128
129 In this study, we set out to investigate the plant apoplastic space as an environment
130 for microbial colonization. We specifically addressed how induced immune responses
131 alter the abiotic and biotic composition of the apoplast. Furthermore, we investigated
132 signatures of microbial adaptation to the apoplastic environment by growth assays of
133 plant-associated microbes in the presence of plant immune compounds. We used
134 wheat as a model system to dissect changes in apoplastic fluid compositions. Wheat
135 is one of the most important crops grown world-wide. In recent years, research has
136 focused on the wheat microbiome considering the putative potential of microbiota-
137 manipulation in plant growth promotion and stress tolerance (e.g., (14-16). In this
138 regard, insights into the dynamics of microbiota composition are scarce, hindering our
139 ability to predict the stability of beneficial microbes in the field.
140
141 In our study, we used wheat as a plant model system to uncover variation in the
142 apoplast environment. Wheat can be infected by the ascomycete fungus
143 *Zymoseptoria tritici*, a hemibiotrophic pathogen that invades leaf tissues via stomatal
144 openings. Several quantitative and qualitative resistance loci have been mapped in
145 wheat using quantitative trait locus analyses and genome wide association studies
146 (17-21). Among these resistance loci the best characterized is *Stb6*, which confers
147 resistance towards *Z. tritici* isolates by the secretion of the AvrStb6 protein (17, 22,
148 23). In resistant wheat varieties harboring *Stb6*, the recognition of AvrStb6 in *Z. tritici*
149 isolates occurs via guard-cell located in the stomata, preventing fungal invasion and
150 colonization (24). Hereby, recognition of *Z. tritici* induces a strong up-regulation of local

151 and systemic defense responses involving the production of ROS and other defense
152 related compounds, as well as lignin accumulation (10). In susceptible wheat however,
153 the fungus efficiently suppresses defense signaling to colonize the mesophyll tissue.
154 In a previous study, we compared the impact of microbiota composition in wheat
155 leaves after inoculation with spores of *Z. tritici* (10). We showed that the fungal
156 pathogen greatly influences microbiota composition in both resistant and susceptible
157 wheat. We speculate that the microbiota composition may change in response to both
158 direct interactions with the fungus as well as indirect effects conferred by the altered
159 apoplast environment.
160
161 An interesting observation is the fact that microbial diversity overall is reduced in a
162 resistant wheat cultivar upon infection with *Z. tritici* (10). The reduced microbial
163 diversity correlates with a strong accumulation of antimicrobial defense metabolites
164 which are induced by the invading pathogen. One component of the microbial
165 community however persists during the pathogen-induced immune response
166 suggesting that these microbes are capable of avoiding or tolerating host immune
167 responses.
168
169 In the present study, we set out to further explore the dynamic of abiotic and biotic
170 conditions in a wheat metaorganism. We notably considered changes in the apoplastic
171 space during pathogen invasion and explored the diversity and adaptations of core
172 metaorganisms members. To this end, we developed a protocol for extraction of
173 apoplastic fluids from wheat leaves. We used the apoplastic fluid samples for
174 proteome analyses and for isolation of the microbial communities inhabiting the
175 particular intercellular space of the wheat mesophyll.

176

177 Our study reveals a highly variable environment, selecting for microbes with particular
178 adaptations. We observed a portion of microbes that are specifically enriched in the
179 resistant cultivar Chinese Spring (which harbors *Stb6*), and we hypothesize that they
180 compose a core microbial community. We further observed that several of these core
181 microbes show antagonism against *Z. tritici* and may therefore also play a role in
182 pathogen defense.

183

184 **Material and methods**

185 **Fungal and plant material**

186 The Dutch *Z. tritici* IPO323 (internally named Zt244) strain producing the effector
187 protein AvrStb6 was used in this study (Wageningen University, Netherlands) (17, 22,
188 25). Additionally, the Zt05 strain isolated in Denmark (26), and Zt10 strain isolated in
189 Iran (27), were used in the *in-vitro* confrontation assays. The fungal cells, stored in
190 glycerol at -80°C, were recovered in 50 mL of YMS medium (yeast malt sucrose broth,
191 4 g/L yeast extract, 4 g/L malt extract, 4 g/L sucrose, pH 6.8) incubated at 18 °C for 4
192 days. The susceptible wheat (*Triticum aestivum* L) cultivar Obelisk (without the
193 resistance gene *Stb6*) was obtained from Wiersum Plant Breeding BV (the
194 Netherlands), and the resistant landrace Chinese Spring (with the resistance gene
195 *Stb6*) was kindly provided by Bruce McDonald from ETH Zürich.

196

197 **Plant growth conditions**

198 Seeds from both Obelisk and Chinese Spring wheat genotypes were surface washed
199 for 5 min with 1x phosphate-buffered saline (PBS; 8 g/L NaCl, 0.2 g/L KCl, 1.44 g/L
200 Na_2HPO_4, 0.24 g/L KH_2PO_4, pH 7.4) supplemented with 0.02% (v/v) of Tween 20,

201 followed by three times (1 min each) with sterile deionized water. Twelve seeds of
202 each wheat genotype were sown in square pots (9 x 9 x 9.5 cm) containing peat soil
203 (HAWITA GmbH, Vechta, Germany). Subsequently, each pot was inoculated with 100
204 mL of agricultural soil slurry by diluting 10 g of soil collected from the experimental
205 farm Hohenschulen (54°18'53.7" N – 9°58'44.1" E) of the Christian-Albrechts
206 University of Kiel in Germany in 1L of sterile deionized water. Plants were grown during
207 the entire experiment in the greenhouse under constant conditions of 16/8 h light/dark
208 cycle at 22°C (day) and 20°C (night) and 80% relative humidity.
209

210 **Fungal infection**

211 Plant inoculations were performed as previously described (28). In brief, the IPO323
212 strain was grown in 50 mL of YMS medium in a rotary shaker for five days at 18°C.
213 After the incubation, blastospore suspensions were filtered through sterile cheesecloth
214 and pelleted at 3750 rpm for 15 min at 4°C. The supernatant was discarded and the
215 cells were resuspended in sterile deionized water. The concentration of the
216 blastospore suspensions were determined using KOVA Glasstic counting chambers
217 (KOVA International Inc., USA) and adjusted to a final concentration of 10^7
218 blastospores/mL in 30 mL of sterile water supplemented with 0.1% (v/v) Tween 20.
219 We sprayed 14-day old plants until run-off and placed for three days in sealed plastic
220 bags to keep humidity at 100%. The plastic bags were then removed, and the plants
221 were kept in the greenhouse until the end of the experiments. Mock-treated plants
222 were sprayed with sterile water. To ensure the success of fungal infection, second
223 leaves of additional infected plants were harvested at 14 days-post inoculation (dpi).
224

225 **Wheat apoplastic fluids extraction**

226 Apoplastic fluids (AFs) was obtained according to the method of R. T. Nakano et al.
227 (29) with slight modifications (Fig. S1A). Ten 1st and 2nd fully expanded wheat leaves
228 were harvested at 8 dpi from plants growing in separated pots. Three biological
229 replicates containing 20 leaves (the 10 first and 10 second wheat leaves) were pooled
230 for the AF extraction. Leaves were surface washed two times (5 min each time) with
231 1x PBS, and 1x PBS supplemented with 0.02% (v/v) of Tween 20, followed by three
232 times (1 min each) with sterile deionized water. The washed leaves were submerged
233 in 400 mL of infiltration buffer (5 mM sodium acetate, 0.2 M calcium chloride, pH 4.3)
234 containing two dissolved cOmplete™ EDTA-free protease inhibitor cocktail tablets
235 (Roche Applied Science, Penzberg, Germany) and vacuum-infiltrated at 900 mbar for
236 10 min. Subsequently, the vacuum was released gently for approximately 30 min. The
237 vacuum step was carried out 2-3 times to reach a maximum saturation of the infiltration
238 buffer in the apoplastic space. The excessive buffer was dried quickly between two
239 sheets of soft paper towel, and the leaves were placed into a 20 mL blunt-end
240 needleless syringe (without the plunger). The syringe was introduced into a 50 mL
241 falcon tube and then centrifuged at 4000 rpm for 4 minutes at 4 °C. The centrifugation
242 step was repeated up to three times to extract a maximum amount of the apoplastic
243 liquid. A summary of the methodology used for the apoplastic fluid isolation is given in
244 Fig. S1A. Two 500 µL aliquots of AFs were lyophilised overnight, followed by
245 resuspension in 200 µL of 100 mM ammonium acetate, and then stored at -20° until
246 required for proteomic or Western blot analyses. Additionally, 1 mL of AFs were kept
247 on ice until plated on different media for microbial isolation.
248
249 **Western blot analysis**

250 Western blotting was performed with three biological replicates of each treatment to
251 identify any contamination of the apoplastic fluid samples by intracellular proteins. The
252 cytoplasmic protein Ribulose-1,5-bisphosphate carboxylase/oxygenase (so-called
253 RubisCO, RbcL) was used as a marker for intra-cellular contamination of the
254 apoplastic fluid samples. Since different eukaryotes colonize the apoplast, including
255 *Z. tritici* for the wheat infected plants, we furthermore used the Histone H3 protein as
256 a general eukaryote positive marker. One microgram of protein from the apoplastic
257 fluids and a quantitative rubisco positive standard control (Agrisera, Vännäs, Sweden)
258 were electrophoretic separated on Mini-PROTEAN TGX Precast Gels (8-16%
259 polyacrylamide, Bio-Rad Laboratories, California, USA) at 70V for 15 min, and then
260 increased to 100V for 60 min, followed by blotting to PVDF membranes (Bio-Rad
261 Laboratories, California, USA). Membranes were overnight blocked with 1x TBS-T
262 (Tris-buffered saline with Tween-20) containing 4% of non-fat dry milk at 4°C with
263 agitation. Blots were then incubated in the primary antibodies against Histone H3 (H3,
264 Agrisera, Vännäs, Sweden) (1:5'000) or RuBisCo large subunit (RbcL, Agrisera,
265 Vännäs, Sweden) (1:10'000) for 1h at room temperature with agitation. After washing,
266 the blots were incubated in 1x TBS-T containing 2% of non-fat dry milk in which the
267 secondary antibodies conjugated to horseradish peroxidase (anti-rabbit, 1:20'000 from
268 Santa Cruz Biotechnology, Dallas, USA; or anti-chicken, 1:25'000 from Agrisera,
269 Vännäs, Sweden) for 1h at room temperature. The blots were detected using ECL-
270 Select Western Blotting detection reagent (Cytiva, München, Germany) according to
271 the manufacture's instruction, and images were obtained using the CCD imager
272 Documentation System (Bio-Rad Laboratories, California, USA).
273
274 **Proteome analysis by liquid chromatography-mass spectrometry (LC-MS)**

275 Protein concentrations in the apoplast samples were determined using the micro BCA
276 assay (Thermo Fischer Scientific, Germany). 50 µg total protein of each sample were
277 reduced with 10 mM dithiothreitol (DTT) at final concentration for 1h at 56°C. Samples
278 were then alkylated with 50 mM Chloroacetamide (CAA) for 30 min at 25°C in the dark,
279 followed by overnight digestion with trypsin (enzyme to protein ratio of 1:100)
280 (Promega, Germany) at 37 °C. Digestion was stopped by acidification using 5% formic
281 acid (FA) and samples were subsequently desalted on a C18 solid phase extraction
282 cartridge (SepPak C18, 1cc, 50 mg) (Waters, Eschborn, Germany) following
283 manufacturer's instructions. Peptides were eluted from the cartridges with 60%
284 acetonitrile (ACN) supplemented with 0.1% trifluoroacetic acid (TFA), and dried via
285 vacuum centrifugation (Concentrator Plus, Eppendorf).
286
287 Dried peptides were resuspended in 3% ACN and 0.1% TFA and then separated
288 employing a Dionex U3000 nanoHPLC system (Dreieich, Germany) equipped with an
289 Acclaim Pepmap100 C18 column (2 µm, 75 µm x 500 mm). The eluents used were
290 eluent A: 0.05% FA, and eluent B: 80% ACN/ 0.04% FA. A programmed 123 min run
291 at 300 nl/min was performed as follows: 2 min at 4% eluent B, 90 min linear gradient
292 4% to 50% eluent B, 5 min linear gradient 50% to 90% eluent B, 10 min at 90% eluent
293 B, followed by equilibration for 16 min at 4% eluent B. Eluted peptides were analyzed
294 online on a QExactive^{TM} Plus mass spectrometer (Thermo, Bremen, Germany). A
295 top15 data acquisition method was applied with a full MS scan (350-1400 m/z,
296 resolution 70,000, AGC 3e6, Max IT 50 ms), followed by HCD fragmentation and
297 MS/MS scans of the 15 most intense ions (NCE 27.5, resolution 17,500, AGC 1e5,
298 Max IT 100 ms). A 20 s dynamic exclusion and a lock mass of 445.12003 were applied.
299 Each sample was injected twice.

300

301 **Proteomic data analysis**

302 MS raw data were analyzed using the Uniprot reference proteomes of *Triticum*
303 *aestivum* (130,673 proteins), *Z. tritici* strain IPO323 (10,972), *Acidovorax sp*. (5,416),
304 *Curtobacterium flaccumfaciens* (3,574), *Pseudomonas anguilliseptica* (4,385),
305 *Pseudomonas rhodesiae* (5,708), *Flavobacterium sp* (3,029) *Plantibacter flavus*
306 (3,813), and known contaminants (cRAP) were determined using the Sequest HT
307 search engine linked to Proteome Discoverer™ 2.5 (Thermo Fischer Scientific,
308 Germany). Enzyme specific was set to Trypsin, and two missed cleavages were
309 allowed. Precursor and fragment ion tolerances were set to 10 ppm and 0.02 Da,
310 respectively. Carbamidomethylation of cysteine was set as a fixed modification and
311 oxidation of methionine as a variable modification. The INFERYS rescoring node was
312 incorporated into the processing workflow. Strict parsimony criteria were applied with
313 1% false discovery rate (FDR) cutoff used for both peptides and proteins. A label-free
314 quantification method, based on the intensities of the precursor ions, was performed
315 using Minora detection with match between runs. Only proteins with high combined
316 FDR confidence were considered. Moreover, *T. aestivum* proteins were filtered to
317 contain at least two identified peptides; proteins of other organisms were considered
318 underrepresented in the samples.

319

320 Protein groups and their respective raw intensities were exported and further analyzed
321 using the software Perseus v.1.6.15.0 (30). For quantitative analysis, intensities of two
322 technical injections per sample were averaged and then normalized by median based
323 normalization. Normalized intensities were $\log_2$ transformed and grouped per
324 condition (*e.g.*, Obelisk Mock or Chinese Spring Mock). Proteins were filtered to

contain at least three values in one group, and imputation of missing values from normal distribution was performed separately for each column (Perseus default values, Width 0.3 and down shift 1.8). Principal component analysis (PCA) plots were generated in Perseus and the volcano graphs were plotted with bioinfokit (31) using a custom made Python script.

Gene enrichment analysis and predictions

Gene ontology (GO) enrichment analysis was performed with the webserver DAVID 2021 (32, 33). All of the identified wheat proteins were searched against the default background and functional annotation charts with GOTERM_BP_DIRECT, GOTERM_CC_DIRECT and GOTERM_MF_DIRECT categories (EASE 0.1). Up to five GO terms with lowest Benjamini Hochberg corrected p-values (<0.05) were plotted. GO enrichment of the differentially expressed proteins in the volcano plots were performed in a similar way; however, identified proteins were used as a background and up to three GO terms with lowest Benjamini Hochberg p-values (<0.05) were plotted for each category.

For prediction of apoplastic proteins, a FASTA file of the identified proteins was analyzed using AploplastP 1.0 (34) and SignalP 6.0 (Organism: Eukarya, Model mode: Fast) (35). Proteins predicted to be apoplastic by the program ApoplastP or having a signal peptide predicted by the SignalP software were considered as predicted apoplastic proteins. Venn diagrams were plotted using Venny 2.1 program (36).

Establishment of a wheat-enriched endophytic community-based culture collection

350 Using the apoplastic fluid samples, we further isolated a collection of bacteria and
351 fungi. The culture collection represents the microbial community which is enriched in
352 the inter-cellular space of wheat leaves. The culture collection was obtained using
353 freshly extracted AFs from mock and IPO323 infected Obelisk or Chinese Spring
354 wheat plants. To optimize the isolation of microorganisms we used a set of different
355 media. 100 µL of both undiluted or 1:10 dilution of AF samples were plated on three
356 different media, including as Trypticase Soy agar (TSA; 7.5 g/L BBL Trypticase Soy
357 Broth (TSB); Becton Dickinson and Company, NJ, USA; 15 g/L agar) used as a non-
358 selective growth medium for bacteria; Reasoner's 2A agar (R2A; 18.1 g/L R2A-Agar;
359 Carl Roth, Karlsruhe, Germany) a medium that favors slow-growing bacteria; and
360 *Pseudomonas syringae* medium (PSM; 15 g/L sucrose, 3.75 g/L peptone, 0.38 g/L
361 K2HPO4, 0.1 g/L MgSO4, 15 g/L agar) recommended to
362 isolate *Pseudomonas* species. Three technical replicate plates were prepared per
363 treatment and media combinations. Plates were incubated for four days at 22°C or
364 until the appearance of visible fastidious colonies. For microbial singularization,
365 individuals exhibiting diversity colony morphotypes (*e.g.,* distinct size, shape, texture,
366 or pigmentation) were transferred onto a new agar plate and incubated for additionally
367 four days at 22°C. This procedure was repeated twice in at similar way. The
368 individualized colonies were then transferred to canonical tubes containing 25 mL of
369 TSB medium and incubated on a rotary shaker at 145 rpm for seven days at 22°C.
370 Finally, cryostocks were prepared by mixing 1 mL of the liquid cultures with 1 mL of
371 50% (v/v) YMS glycerol medium.
372
373 **DNA extraction, species identification and phylogenetic analysis**

374 Cells of individualized colonies were scratched from the agar and dissolved in 250 µL
375 of sterile deionized water. 50 µL of the cell suspensions were lysed by adding 100 µL
376 of TE lysis buffer (1 mM EDTA and 10 mM TrisHCl, pH 8 + 0.1 % Triton X 100) and
377 incubated at 99 °C for 10 min. Subsequently, the samples were centrifuged at 13'000
378 *x g* for 10 min. The supernatant was transferred to a new tube and used as DNA
379 template for PCR amplification. In order to identify the bacterial or fungal species,
380 PCRs using the partial 16S rRNA and the ITS (internal transcribed spacer) regions
381 were conducted, respectively (37, 38). The 16S rRNA V3-V7 gene region was PCR-
382 amplified (94°C/2 min; 94°C/30 sec; 57°C/30 sec; and 72°C/1 min for 25 cycles, and
383 final extension 72°C/10 min) using the forward primer 341F (5' - CCT ACG GGA GGC
384 AGC) and the reverse primer 1192R (5' - ACG TCA TCC CCA CCT). Additionally, the
385 ITS region was PCR-amplified (95°C/2 min; 95°C/30 sec; 55°C/30 sec; and 72°C/20
386 sec for 25 cycles, and final extension 72°C/10 min) using the forward primer ITS1F (5'
387 - CTT GGT CAT TTA GAG GAA GT) and the reverse primer ITS1R (5' - GCT GCG
388 TTC TTC ATC GAT GC). The PCR products were purified using the Wizard™ SV Gel
389 and PCR Clean-Up System (Promega, Madison, WI, USA) following the manufactures
390 instructions. The obtained purified PCR products were submitted for Sanger
391 sequencing (Institute of Clinical Molecular Biology, Kiel, Germany) using the
392 abovementioned forward primer sequences. To identify the microbial species, the
393 nucleotide sequences were analyzed using the SILVA database with the incorporated
394 SILVA ACT service (39) for homology searches, sequence alignment and taxa
395 identification. Furthermore, individual sequences were blasted against the NCBI
396 (National Center for Biotechnology Information) database. The nucleotide sequences
397 were aligned using MEGA software (40). The best-fit model of nucleotide evolution
398 was the GTR+G also determined by MEGA. The phylogeny reconstruction was

computed by maximum likelihood (ML) using 500 bootstraps using RAxML program (41).

Jaccard similarity index and phylogenetic analysis

The β-diversity (variation between treatment groups) was measured using the non-phylogenetic-based approach Jaccard index (42). Jaccard is a qualitative index that utilizes the presence-absence data of the species, as follows: the S_i, S_j, and S_{ij} denote the number of species (OTUs) present in Samples *i*, *j*, and both *i* and j samples, respectively, the Jaccard distance between Sample *i* and *j* is represented as: $Jac_{(i,j)} = \frac{Si+Sj}{Si+Sj+Sij}$. Distance matrices were constructed based on the percentage of dissimilarity of community-based culture collection.

A dataset containing the nucleotide sequences of all identified species was used for phylogenetic analysis. The two fungal species *Rhizopus arrhizus* and *Mucor kunryamgriensis* from the Mucoroycota were used as outgroups. The best-fit model of nucleotide evolution was the GTR+G model determined by MEGA v.11 (40). The nucleotide alignment was performed in MEGA v.11 using the Clustal W multiple sequence alignment (43), followed by a Maximum Likelihood method for phylogenetic reconstruction using 500 bootstraps performed in the RAxML v.8 (41, 44). The graphic display of the phylogenetic tree was adapted with the online tool iTOL v.5 (45).

Confrontation assays

The potential antagonistic activities among the wheat-enriched endophytic microbes and *Z. tritici* were accessed by confrontation of co-cultures on Petri dishes. Considering the extensive genetic variation in *Z. tritici*, we included additionally two *Z.*

424 *tritici* isolates in the assay allowing us to identify general and isolate-specific
425 interactions of *Z. tritici* with wheat microbiome members. In addition to the Dutch
426 isolate IPO323, we included two additional field isolates of *Z. tritici;* Zt05 from
427 Denmark, and Zt10 from Iran both isolated from wheat (46).
428
429 To evaluate the antagonistic activity of the wheat-associated microbes against *Z. tritici*,
430 the blastosporulation of the three tested *Z. tritici* strains was recovered on 50 mL of
431 YMS liquid medium incubated at 18°C for six days. The 20 mL of soft agar medium
432 was prepared using 15 mL of sterile deionized water, 5 mL of boiling Fries 3 agar
433 medium supplemented with trace elements (as previously described), and fungal
434 inoculum which gives a final concentration of 1.88×10^5 blastospores/mL. The wheat-
435 associated microbes were then recovered in Fries 3 liquid medium for three or four
436 days before the assays on a rotary shaker (200 rpm) at 23°C. Microbial cell densities
437 were measured and adjusted to OD^{600} of 0.2 at 600 nm. Finally, drops of 3.5 µL of
438 each tested wheat endophyte were spotted onto three independent Fries 3 plates
439 amended with *Z. tritici* spores. Plates containing solely Fries 3 medium were used as
440 control. Nine different isolates placed 3.5 cm apart were tested per Petri dish. Each
441 isolate was tested three times on independent plates. 1.5 µL of Hygromycin B (at a
442 final concentration of 19.61 mg/L) was used as positive control for fungal growth
443 inhibition. Plates were incubated in the dark at 23 °C and photographed after three or
444 four days of incubation. Digital images were processed using the ImageJ software (47)
445 for the quantification of the inhibition zones. A Kruskal-Wallis test was performed to
446 determine the differences between the size of inhibition for the three tested *Z. tritici*
447 strains. The Dunn's test was then used to define the significance difference between
448 each independent group. The association between the percentage of isolates that

449 shown growth promotion or inhibition by each tested *Z. tritici* strain and the treatment
450 from where the wheat-associated microbes were isolated was examined using
451 Fisher's exact test.
452
453 **Response to plant immune-related compounds**
454 To investigate adaptations of the endophyte to the apoplastic environment, we
455 conducted an *in vitro* assay with different plant-stress related molecules. We included
456 both bacteria and basidiomycete yeasts in the assay. Hydrogen peroxide (H_2O_2) and
457 three different secondary metabolites, including cinnamyl alcohol (CA), quinic acid
458 (QA), and nonanoic acid (NA) were used to determine the tolerance of the wheat-
459 associated microbes to plant immune responses. H_2O_2 accumulates in the apoplast
460 and is widely used to mimic ROS burst upon Microbe-Associated Molecular Patterns
461 (MAMPs) perception (48): CA, QA, and NA were previously demonstrated to be highly
462 abundant in the Chinese Spring, but not in Obelisk upon *Z. tritici* infection (49). We
463 consider these metabolites to be defense-related metabolites which are induced
464 specifically in *Z. tritici* resistant wheat. To test for microbial tolerance, the microbes
465 were recovered in Fries 3 liquid medium (5 g/L $C_4H_{12}N_2O_6$, 1 g/L NH_4NO_3, 0.5 g/L
466 $MgSO_4$*$7H_2O$, 1.3 g/L KH_2PO_4, 2.6 g/L K_2HPO_4, 1 g/L yeast extract, 30 g/L sucrose)
467 for 24h on a rotary shaker (200 rpm) at 23°C. Microbial cell densities were measured
468 and adjusted to OD^{600} of 0.2 at 600 nm. The ROS assays were performed on Fries 3
469 agar plates (16 g/L agar) supplemented with 2 mL of trace elements (167 mg/L LiCl,
470 227 mg/L $CuSO_4.5H_2O$, 34 mg/L H_2MoO_4, 72 mg/L $MnCl_2.4H_2O$, 80 mg/L
471 $CoCl_2.6H_2O$). Drops of 3.5 µL of each tested wheat endophyte were plated on three
472 independent Fries 3 plates amended with 0.5, 1, or 2 mM of H_2O_2. Plates containing
473 only Fries 3 medium were used as control. Plates were incubated 23 °C and

474 photographed at 5 dpi. The colony diameter was calculated from digital images of
475 colonies formed in three independent Petri dishes using ImageJ software (47). The
476 percentage of growth inhibition or promotion in response to the presence of H_2O_2 was
477 calculated based on the colony diameter of the colonies growing on control plates.
478 These percentages were then plotted in a bubble plot using ggplot2 package from R
479 (50).
480
481 The plant secondary metabolite assays were conducted on microtiter plates containing
482 200 µL of Fries 3 liquid medium supplemented with trace elements and 1 mg/mL at
483 final concentration of CA, or 4 mg/mL at final concentration of NA or QA (all
484 compounds from Sigma, Missouri, USA). The doses were pre-defined in a previous
485 experiments using 10 microbial strains (data not shown). The secondary metabolites
486 CA and NA were solubilized in ethanol, while QA was dissolved in dimethyl sulfoxide
487 (DMSO). Therefore, microtiter wells containing solely Fries 3 medium and Fries 3
488 supplemented with ethanol or DMSO were used as controls. Each tested wheat
489 endophyte was adjusted to a final OD^{600} of 0.1. Eight and twelve technical replicates
490 were performed for the controls and each secondary metabolites per microbial strains,
491 respectively. Plates were incubated on a rotary shaker (190 rpm) at 23°C and OD^{600}
492 measurements were taken after 24, 48, 72, 96 and 168h of incubation. The growth
493 ratio of each microbial strain was assessed by dividing the mean OD in the presence
494 of each secondary metabolite by the mean OD of the corresponding control culture at
495 each time point. This ratio represents the relative growth of microbial strains in the
496 presence of CA, NA, and QA compared to the control. An OD ratio $\geq$ 1.1 indicates that
497 the compound promoted microbial growth, while OD ratio $\leq$ 0.9 suggests that the
498 compound inhibited the microbial growth. We considered stable bacterial growth if the

499 OD ratio between 0.9 and 1.1. The histogram containing the relative growth ratio
500 distribution was plotted using ggplot2 in R (50). The number of microbial strains
501 showing growth promotion, inhibition, or non-affected growth (ratio between 0.9 and
502 1.1) in the presence of each secondary metabolite and time point were plotted in an
503 alluvial plot using ggplot2 in R (50).
504
505 **Results**
506 **LC-MS/MS analyses reveal qualitative and quantitative effects of *Z. tritici***
507 **infection on the wheat apoplastic proteome**
508 To identify the proteins expressed during the compatible and incompatible
509 interactions, we firstly conducted an infection assay with the susceptible wheat cultivar
510 Obelisk (without the resistance gene *Stb6*) and the resistant landrace Chinese Spring
511 (with the resistance gene *Stb6*) inoculated with the IPO323 *Z. tritici* strain, which
512 produce the effector protein AvrStb6 (17, 22, 23, 51). We isolated the apoplastic fluids
513 at 8 dpi, which represents the onset of more extensive fungal intracellular growth, but
514 still at the symptomless biotrophic phase (46, 52). We then confirmed the success of
515 infection at 14 dpi by showing that the IPO323 strain was able to infect and reproduce
516 in leaves of Obelisk, but the infection was aborted in leaves of the resistant Chinese
517 Spring (Fig. S2), corroborating with previous studies (10, 17, 22, 46).
518
519 In order to unveil the proteins involved in the wheat immune response against *Z. tritici*,
520 we applied a bottom-up proteomic analysis on the apoplastic fluid extracts (Fig. 1A).
521 A total of 2’455 protein sequences (Fig. S1B, Fig. 1A, and Table S1) were identified,
522 of which 956 (39%) were predicted as apoplastic proteins using SignalP 6.0 and
523 ApoplastP 1.0 (Fig. 1A). Although RuBisCo was not detected in the apoplastic fluids

524 using Western blot analysis (Fig. S1D), it is not surprising that cytosolic proteins such
525 as ribosomal, mitochondrial and chloroplast proteins were identified due to the high
526 sensitivity of the LC-MS/MS approach (Table S2). Some proteins that were not
527 predicted as apoplastic might be secreted by non-conventional secretion mechanisms.
528 Moreover, non-apoplastic proteins may be critical components of plant cells and play
529 a variety of role in plant growth, development, and stress responses (53-55), thus we
530 included these proteins in the further analysis.
531
532 ***Z. tritici* infection causes substantial change in the apoplastic proteome of the**
533 **susceptible wheat genotype**
534 We compared the proteome data of Obelisk and Chinese Spring to identify the
535 differences between genotypes and between mock-treated and pathogen-infected
536 plants. The wheat genotypes explained the major difference as seen in the PCA plot
537 (Fig. 1B). Intriguingly, when comparing mock-treated and infected plants, we found
538 that fungal infection did not cause a large shift in the Chinese Spring apoplast
539 proteome, but it resulted in a substantial change in the Obelisk cultivar (Fig. 1B).
540
541 We further performed pairwise comparisons to identify the differentially abundant
542 proteins in Obelisk and Chinese Spring plants during fungal infection. To this end, we
543 assessed the fold-change of protein accumulation by comparing the mock-treated and
544 IPO323 infected samples from the same wheat genotype. A total of 248 and 87
545 proteins were higher in abundance in the infected Obelisk and Chinese Spring,
546 respectively (Table S2). On the other hand, 305 and 46 proteins showed a higher
547 abundance in mock treated apoplast of Obelisk and Chinese Spring, respectively
548 (Table S2). Of the measured proteins in Obelisk, about 36% showed a down-

549 regulation in *Z. tritici*-infected samples (242 proteins, Obelisk mock vs infected), while
550 only 13% of proteins in Chinese Spring were down-regulated in the *Z. tritici* infected
551 leaves (86 proteins, Chinese Spring mock vs infected) (Table S2). We hypothesize
552 that these results reflect the extensive physiological and cellular changes which are
553 caused by colonization of *Z. tritici* in the apoplastic space of the susceptible wheat. In
554 Chinese Spring, hyphae of *Z. tritici* do not extent further than the substomatal cavity.
555

556 **Proteomic analysis unveils conserved defense-related signatures in *Triticum***
557 ***aestivum* against *Z. tritici* infection**

558 We next aimed to identify common defense proteins associated with *Z. tritici* infection.
559 We compared the proteins in the two wheat genotypes which showed different
560 abundance in the presence of *Z. tritici*, a total of 673 proteins. We identified a set of
561 24 upregulated proteins shared between infected Obelisk and Chinese Spring plants
562 (Fig. 1C and Table S3). These proteins are predicted to have different biological roles,
563 as cell wall components (*e.g.,* expansins, leucine-rich-repeat extensins, and pectin
564 acetylesterases), in carbohydrate metabolism (*e.g.,* thiamine thiazole synthase and
565 beta-fructofuranosidase), in lipid metabolism (*e.g.,* non-specific lipid transfer proteins
566 (ns-LTPs) and GDSL esterase/lipase), as proteases (*e.g.,* aspartyl protease), and as
567 catalytic enzymes (*e.g.,* peptidases and peroxidases), and as proteins involved in key
568 processes of plant defense responses, such as the cysteine-rich receptor-like kinase
569 (CRK) and leucine-rich repeat (LRR) motif-containing protein. The two identified CRK
570 proteins harbor a Stress-antifungal domain, which is an extracellular domain that
571 consists of the conserved cysteine-rich motif (C-X8-C-X2-C) that possesses antifungal
572 and salt-stress responsive activities (56, 57). Additionally, in plants LRR domains are
573 well-known to be involved in protein-protein interactions, as well as in development

574 and defense processes (58). We conducted a blastp analysis to further predict the
575 functional relevance of the proteins. Hereby we find that the LRR-motif-containing
576 proteins are, polygalacturonase-inhibiting protein (PGIPs) containing LRR-motifs.
577 PGIPs were previously shown to be involved in defense against fungi by inhibiting the
578 activity of polygalacturonases, enzymes secreted by fungal pathogens to degrade
579 pectin in the plant cell wall. Interestingly, pectin degradation by polygalacturonases
580 leads to an accumulation of short-chain oligogalacturonides (OGs) that may be
581 recognized as damage-associated molecular patterns (DAMPs) and elicit plant
582 defense responses (59, 60).
583
584 We performed Gene ontology (GO) enrichment analysis on the significantly different
585 proteins (mock vs infected) in Chinese Spring and Obelisk (Fig. 1D-G), and found that
586 six out of seven previously described ns-LPTs (protein IDs A0A3B6AZK3,
587 A0A3B6C6Z8, A0A3B6EM77, A0A3B6RLW5, A0A3B6SLE4, V9I0Q4, Table S3) were
588 annotated to the GO term systemic acquired resistance (SAR) (Tables S4). The role
589 of ns-LTPs in SAR relates to their participation in the intercellular transport of lipids,
590 which serves as crucial signaling molecules in the induction and propagation of
591 defense responses (61). We also pinpoint that the fungus causes a significantly
592 increase in several stress/defense-related proteins in the susceptible Obelisk including
593 endo-chitinases and chitinases (GO cell wall and chitin processes), Bowman-Birk type
594 proteinase inhibitor B5, pectin acetylesterases, Nepenthesin-like aspartic proteinases,
595 and expansins (GO extracellular region), glucan-endo-1,3-beta glucosidase (GO
596 plasma membrane component), peroxidases (GO extracellular region and plant-type
597 cell wall), serine carboxypeptidase (GO serine-type carboxypeptidase activity) (Figs.
598 1D-F and Table S4). Interestingly, the resistant Chinese Spring also show an increase

599 in the abundance of expansins and peroxidases (GO extracellular region) (Table S4),
600 but the set of proteins is different from Obelisk as we also find an enrichment of
601 proteins of another category of ns-LTPs (GO lipid transport and integral component of
602 membrane), defensins and thaumatin (GO defense response), aspartyl proteases (GO
603 extracellular region and aspartic-type-endopeptidase activity), and GDSL
604 esterase/lipase proteins (GO hydrolase activity) (Figs. 1E-G and Table S4). In
605 summary, our proteome data provide a conserved protein catalog associated with an
606 immune response of *Triticum aestivum* against *Z. tritici* infection, and thereby a novel
607 set of proteins to be functionally validated in future studies.
608

609 **Impact of fungal infection on the photosynthesis apparatus and general plant**
610 **physiological processes**

611 We found that *Z. tritici* infection strongly impacts the abundance of proteins associated
612 with plant physiological processes. First of all, we observed a downregulation of
613 proteins involved in ribosome biogenesis (*e.g.,* 40S and 60S ribosomal proteins) in
614 both Obelisk and Chinese Spring infected plants (Figs. 1E-G and Table 5). The
615 interferences in the translation machinery may be attributed to several direct and
616 indirect consequences of fungal infection, including the activity of fungal effector
617 molecules that may directly target ribosome functions and reduce overall translation
618 (62-64); or it may be attributed to hormone signaling pathways (*e.g.,* salicylic acid and
619 jasmonic acid) involved in defense responses but also affecting ribosomal protein
620 expression (65). Additionally, the downregulation of 40S and 60S ribosomal proteins
621 may be caused by the reallocation of resources involved in the synthesis of specific
622 defense-related proteins and other components necessary for combating the fungal
623 infection (66). We also observed that *Z. tritici* infection interferes with photosynthesis

624 processes in the susceptible Obelisk wheat (Figs. 1D-F and Table S5). During this
625 compatible interaction, we observed the downregulation of the 30S and 50S
626 chloroplast ribosomal proteins, and proteins involved in chloroplast thylakoid luminal,
627 photosynthesis I and II (*e.g.,* PsbP-like proteins) Figs. 1D-F and Table S5. Contrarily,
628 the presence of the *Z. tritici* does not affect the expression of photosynthesis-related
629 proteins in the Chinese Spring (Figs. 1D-F and Table S5). This finding aligns with a
630 previous study demonstrating that the interaction between AvrStb6 and Stb6 proteins
631 in resistant wheat preserves the efficacy of the photosynthesis apparatus (24). Our
632 findings provide novel evidence for the impact of *Z. tritici* on basal physiological
633 processes, beyond defense, in the infected plant tissue during biotrophic colonization
634 of the fungus.
635
636 **Apoplast proteome data reveals three novel *Z. tritici* proteins as candidates to**
637 **fungal biology and pathogenesis regulation**
638 Although several peptides match to protein sequences of the pathogen databases, we
639 consider it more likely that identified peptides have a plant origin. This is due to the
640 fact, that the amount of plant biomass during biotrophic colonization is much higher
641 than the amount of fungal biomass. Despite this, we successfully identified three
642 proteins with peptides exclusively matching the *Z. tritici* database (Table. S6). The
643 absence of N-terminal signal peptides in both proteins (35), may suggest that they
644 either were extracted from *Z. tritici* cells during in the apoplastic fluid or that they are
645 proteins secreted by the fungus by non-conventional secretion mechanisms. The three
646 fungal proteins include a chorismate synthase (Zt09_12_00295) and a
647 cryptochrome/photolyase (Zt09_1_00976) protein, which are both upregulated in
648 Obelisk. The cryptochrome/photolyase protein is also upregulated in Chinese Spring.

649 The gene encoding the cryptochrome/photolyase protein has previously been
650 identified as a pathogenicity related factor, as it found to be significantly upregulated
651 in an RNA-seq-based transcriptome dataset of IPO323 strain infecting another
652 susceptible wheat cultivar, 'Riband' (67). Analysis of the protein sequence by
653 EffectorP 3.0 (68) predicts cryptochrome/photolyase protein to be a cytoplasmic
654 effector further suggesting a relevance of the protein for host infection. The third fungal
655 protein that we identified, belongs to the glycoside hydrolase family 5
656 (Zt09_11_00165), and was found to be downregulated during fungal infection in
657 Obelisk. Further functional studies are required to elucidate the potential roles of these
658 three novel proteins during the wheat-*Z. tritici* interaction.
659

660 **Isolation and characterization of wheat-apoplast microbial communities in**
661 **Chinese Spring and Obelisk**

662 Above we show that *Z. tritici* infection triggers the secretion of various proteins with
663 antimicrobial properties. These proteins may directly impact the microbial community
664 residing within the wheat apoplastic space. Moreover, the recognition of DAMPs or
665 microbe-associated molecular patterns (MAMPs) within the apoplast compartment
666 can activate pattern-triggered immunity (PTI) and/or effector-triggered immunity (ETI),
667 and these immune responses may also promote the biosynthesis of plant metabolites
668 and compounds possessing antimicrobial activity. Thus, we next hypothesized that
669 these immune-related proteins/compounds could have a direct and/or indirect effect
670 on the plant-associated microbiota leading to the prevalence of specific microbial taxa
671 that tolerate wheat defense responses. To test this hypothesis, we firstly cultured and
672 purified microbial isolates from the apoplastic fluids of mock-treated and IPO323
673 infected Obelisk and Chinese Spring wheat plants (Fig. S1C-D). In total, we picked

674 667 isolates cultured from PSM (n= 221, 33.1%), R2A (n= 225, 33.7%), and TSA (n=
675 221, 33.1%) (Fig. 2A), suggesting a similar cultivation success for the different media.
676 The wheat-enriched endophytic community-based culture collection is composed of
677 188 purified and archived isolates which we also classified taxonomically using 16S
678 rRNA gene sequencing (Table S7). The 16S rRNA data allowed us to group strains
679 belonging to the same species. Thereby we find that the collection represents 59
680 species from 21 bacterial families in the phyla Actinobacteria (n= 42; 13 species),
681 Bacteriodetes (n= 8; 6 species), Firmicutes (n= 1; 1 specie), and Proteobacteria (n=
682 124; 36 species). We also isolated fungi including Ascomycetes (n= 9; representing
683 the re-isolation of *Z. tritici* from Obelisk and Chinese Spring infected plants) and
684 Basidiomycetes (n= 4; 3 species) (Figs. 2A-B and D, and Table S7). Importantly, *Z.*
685 *tritici* was exclusively re-isolated from infected Obelisk and Chinese Spring plants,
686 confirming i) the presence of *Z. tritici* in the apoplast of infected plants and ii) the
687 absence of cross-contamination between mock and inoculated plants. Overall, the
688 predominant phyla in the culture collection were Proteobacteria (65.9%), followed by
689 Actinobacteria (22.3%), Ascomycetes (4.7%), Bacteroidetes (4.2%), Basidiomycetes
690 (2.1%), and Firmicutes (0.5%).
691
692 ***Z. tritici* infection does not affected microbial species richness in resistant host,**
693 **but leads to more stochastic microbial communities in a susceptible host**
694 A previous study showed that IPO323 infection promoted a significant reduction in
695 community richness in Chinese Spring, but the fungal infection had no significant effect
696 on community composition of the susceptible cultivar Obelisk (10). With our culture-
697 based approach we obtain a similar number of OTUs (23) from mock- and *Z. tritici*
698 infected Chinese Spring plants. For Obelisk we isolated 14 and 17 OTUs from mock

699 and *Z. tritici* infected plants, respectively. Although, the culture-based approach does
700 not provide the complete diversity of apoplast-associated microbes, we considered
701 the culture collections as proxies for the complete diversity. Hereby, we compared the
702 composition of microbes isolated from the different conditions and used the Jaccard
703 index (JI) to compare the dissimilarity between microbial communities based on their
704 species richness (Fig. 2C). Comparing the effects of *Z. tritici* infection in the two wheat
705 genotypes, we find the highest dissimilarity between Chinese Spring-mock and
706 Chinese Spring-infected microbial communities (JI=0.86) The dissimilarity between
707 Obelisk mock and infected communities was considerably lower (JI=0.91). This
708 observation is in agreement with our previous study which likewise showed the
709 strongest impact of *Z. tritici* infection in the resistant wheat Chinese Spring (10). This
710 observation correlated with an excess of defense related metabolites in pathogen
711 infected leaves.
712
713 **Identification of core microbes which show increased resilience to wheat**
714 **defense responses**
715 The microbes recovered from mock-treated Obelisk plants showed a predominance
716 of Proteobacteria (70.3%), followed by Actinobacteria (24.3%) and Bacteroidetes
717 (5.4%). However, a distinct shift in microbial composition was observed in infected
718 Obelisk plants, with Actinobacteria dominating 60.4%, while Proteobacteria accounted
719 for only 11.6%. Actinobacterial species have been extensively studied for their plant-
720 beneficial roles in disease suppression and as keystone taxa in plant microbial
721 communities (69-72). Within our culture collection, all Actinobacterial representatives
722 belonged to the *Microbacteriaceae* family; however, we observed variations at the
723 genus level between mock-treated and infected Obelisk plants. While *Curtobacterium*

724 and *Leifsonia* were identified in mock-treated plants, infected Obelisk plants were
725 colonized by the genera *Curtobacterium*, *Kineococcus*, *Frigoribacterium*,
726 *Microbacterium*, and *Plantibacter*. Interesting, when comparing the associated
727 microbes of Obelisk, we found that *Curtobacterium* and *Sphingomonas* were the only
728 genera recovered from both uninfected and infected (Fig. 2B), suggesting their
729 resilience to the plant defense responses triggered by *Z. tritici* infection in this
730 susceptible wheat cultivar or the antimicrobial compounds produced by the fungus
731 itself.
732
733 We next evaluated the recovered microbial communities associated with Chinese
734 Spring (Fig. S3 and Table S7). Proteobacteria was the most predominant phylum in
735 both mock-treated (83.7%) and infected (81.3%) plants, followed by Actinobacteria
736 (8.1% and 11.8%, respectively) and Bacteroidetes (8.1% and 3.4%, respectively).
737 Additionally, the phylum Firmicutes (1.7%) was identified solely in Chinese Spring
738 infected plants. When comparing Proteobacteria at the genus level, *Pseudomonas*
739 was the predominant genus in both mock-treated and infected plants (60.9% and
740 79.1%, respectively). As a point of comparison, *Pseudomonas* species accounted for
741 53.8% of the recovered microbiota from mock-treated Obelisk plants compared to only
742 20% in this susceptible cultivar infected with *Z. tritici*. Finally, by comparing the
743 associated microbes of Chinese Spring, we found that *Curtobacterium*, *Acidovorax*,
744 and *Pseudomonas* were the three genera recovered from both uninfected and infected
745 plants (Fig. 2B), indicating their resilience to the plant defense responses triggered by
746 *Z. tritici* infection in this resistant wheat genotype or the antimicrobial compounds
747 produced by the fungus itself. In summary, *Z. tritici* infection in the susceptible host
748 resulted in a shift towards Actinobacteria dominance and a decrease in Proteobacteria

749 members, while *Pseudomonas* predominated in other host conditions. These findings
750 highlight the interplay between host susceptibility and microbial community
751 composition, underscoring the potential importance of Actinobacteria and
752 *Pseudomonas* in plant defense responses and disease outcomes.
753
754 **Microbial *in-vitro* confrontation assays identify antagonists of *Z. tritici* in the**
755 **wheat apoplast**
756 We next sought to characterize the interaction response of recovered microbes and
757 *Z. tritici* in an in vitro assay. Briefly, we conducted confrontation co-cultures to explore
758 the antagonistic potential of wheat endophytic microbes against three geographically
759 distinct *Z. tritici* isolates, including the Dutch isolate IPO323, the Danish Zt05, and the
760 Iranian Zt10. Scheme illustrating the plates is shown in Fig. 3A, and the overall
761 inhibitory phenotypes summarized in Figs. S4-6.
762
763 Six wheat-associated microbes did not show visible growth (*e.g.,* Fig. 3B), and were
764 therefore excluded from the analysis. In general, we did not observe any substantial
765 difference in the inhibitory activity among fungal isolates suggesting that sensitivity
766 and tolerance to plant-associated bacteria overall are conserved mechanisms in *Z.*
767 *tritici*, at least under the conditions tested here (Fig. 3C and S7A). The assay revealed
768 an inhibitory effect in 15 out of 72 microbes against at least one of the tested *Z. tritici*
769 isolates. Twelve isolated inhibited all the three *Z. tritici* isolates, while the
770 *Paraoerskovia marina* affected negatively the growth of Zt05, and *Variovorax*
771 *beijingensis* and *Pseudomonas fluorescens* inhibited growth exclusively for Zt10.
772 Although the size of inhibition zones greatly ranged from 21 cm^2 for *Pseudomonas*
773 *brassicacearum* to 0.09 cm^2 for *Paraoerskovia marina*, we found no statistical

774 differences for the size of inhibition zones among the three *Z. tritici* isolates for the
775 individual bacterial associations (Fig. 3C and S7A).
776
777 We further asked whether the antagonistic interactions with *Z. tritici* included specific
778 microbial families. Among the 19 microbial families representing the members from
779 wheat-associated microbes, six families were capable of inhibiting at least one of the
780 *Z. tritici* strains, such as *Comamonadaceae*, *Cellulomonadaceae*,
781 *Pseudomonadaceae*, *Rhizobiaceae*, *Weeksellaceae*, and *Yersiniaceae*, the
782 *Pseudomonadaceae* being the most prevalent inhibitory bacterial family. Other less
783 represented families, such as *Yersiniaceae* and *Weeksellaceae*, also caused strong
784 *Z. tritici* growth inhibition (Fig. 3E). We also find that a significant majority of the
785 microbes inhibiting the three tested *Z. tritici* isolates are gram-negative bacteria (Fig.
786 S7B). Interestingly, we noticed a pattern in the proportion of antagonistic microbes
787 based on the wheat genotype and infection condition from which they were isolated.
788 Microbes isolated from the infected susceptible Obelisk plants were the lesser
789 inhibitors of *Z. tritici* compared to the other treatments (Fig. 3D). In fact, only
790 *Pseudomonas fluorescens* inhibited Zt10, while none of the microbes isolated from *Z.*
791 *tritici*-infected Obelisk inhibited Zt05 or IPO323. Contrarily, the significant proportions
792 of antagonistic microbes were isolated from both mock-treated Obelisk and Chinese
793 Spring, and from the incompatible interaction (Fig. 3D). Here, we identified wheat
794 endophytic microbes with antagonistic potential against different *Z. tritici* isolates,
795 suggesting the necessity of further investigation to elucidate their specific mechanisms
796 in controlling fungal growth.
797
798 **Effect of defense-related plant compounds on apoplast-associated microbes**

799 The defense response of plants to biotic stresses includes the production of ROS and
800 defense-related secondary metabolites. While triggered by pathogenic microbes, the
801 plant defense response may also impact the diversity of commensal microbes
802 colonizing plant tissues (73). To investigate the specific adaptations of the apoplast
803 microbes isolated from Obelisk and Chinese Spring, we phenotyped 69 microbes,
804 including the pathogen *Z. tritici*, for their tolerance or susceptibility to four
805 representative exogenous sources of plant defense compounds (H_2O_2, CA, QA, and
806 NA). The phenotyping consisted of growth measures (i) on solid medium at a single
807 timepoint and (ii) in microtiter plates over a time series.
808
809 In the first assay based on microbial growth on solid medium amended with H_2O_2, we
810 found a significant variation in growth across different bacterial genera and species
811 (Fig. 4). For example, all members from the genera *Acidovorax* and *Brevundimonas*
812 were fully inhibited at 0.5 μM of H_2O_2, while bacteria belonging to the genera *Rahnella*
813 and *Enterobacter* only were inhibited at 1 μM. All tested microbes were inhibited at 2
814 μM, except for *Z. tritici* and one *Pseudomonas anguilliseptica* (AF0034) isolated from
815 mock-treated Obelisk plants. Genes associated with increased tolerance to H_2O_2 were
816 previously identified in *Z. tritici* based on a GWAS study (74); but the ROS-scavenging
817 mechanism for *P. anguilliseptica* remains unknown. Furthermore, we also observed
818 within species variation in the tolerance levels to H_2O_2 including a comparison of
819 different strains of *Pseudomonas spp.* and *Flavobacterium spp.* (Fig. 4). While the
820 growth of *Pseudomonas anguilliseptica* or *Flavobacterium hydatis* were promoted at
821 0.5 and 1 μM, the *Pseudomonas brassicacearum* and *Flavobacterium pectinovorum*
822 were inhibited at 0.5 μM (Fig. 4). Interestingly, strains of Actinobacteria showed a
823 higher tolerance to H_2O_2 by showing either a slight growth promotion or a slight

824 inhibition compared to the rest of the wheat-associated microbes Fig. 4). In our study,
825 the majority of Actinobacterial strains were obtained from Z. tritici-infected Obelisk
826 leaves (Fig. S3B). This observation indicates a more efficient, and potential adaptive,
827 ROS-scavenging mechanism in Actinobacteria allowing these bacteria to cope with
828 the oxidative stress induced during *Z. tritici* infection. Finally, the fungal isolates also
829 displayed high tolerance to H_2O_2. Our assay included fungal species belonging to the
830 genera *Apiotrichum*, *Cystobasidium*, and *Vishniacozyma*. The enhanced ability of
831 fungi to tolerate oxidative stress is known to be attributed to their intricate antioxidant
832 machinery and repair mechanisms, enabling them to survive in environments with high
833 oxidative potential (74-77)
834
835 In the second assay, we determined microbial growth based on estimates from
836 microtiter plates. Hereby, we assessed the impact of CA, QA, and NA on microbial
837 growth. Also, we measured growth promotion, growth inhibition and no-effect on
838 growth across all 69 apoplast-associated microbes over five timepoints (24, 48, 72, 96
839 and 168 hours). Considering the entire course of the experiment, each of the 69
840 microbes were evaluated five times, resulting in 345 measurements. We initially noted
841 a variation in the frequency of microbial isolates that showed inhibition, promotion and
842 stable (no change compared to control) phenotypes across compounds and
843 timepoints (Fig. 5 and Table S8).
844
845 Overall, the compound CA exhibited the highest levels of inhibition with 86% of the
846 measurements showing a growth inhibition (297 inhibitions out of 345), followed by
847 NOA with 67,8% of measurements (234 inhibitions out of 345), and QA with the lowest
848 levels of inhibition, 46,3% (160 inhibitions out of 345) (Fig. 5 and Table S8). These

849 observations were consistent across all time points with the compound CA displaying
850 the highest levels of inhibition (Fig. 5 and Table S8). Interestingly, we highlight intrinsic
851 differences of individual microbes to the three tested compounds, whereas a given
852 individual may show inhibition or promotion of growth according to different
853 compounds.
854
855 We next investigated in more detail how individual microbes varied in susceptibility to
856 each compound overtime (from 24 to 168 hours post incubation). For CA,
857 *Pseudomonas kilonensis* (AF0006), *Enterobacter sp* (AF0002), and *Curtobacterium*
858 *oceanosedimentum* (AF0066) exhibited more growth promotion than any other strain,
859 while *Sphingobium bisphenolicum* (AF0048), *Agrobacterium tumefaciens* (AF0129),
860 *Acidovorax sp* (AF0089), *Pseudomonas sp* (AF0130), *Brevundimonas sp* (AF0072),
861 and *Pseudomonas brassicacearum* (AF0120) were the most inhibited strains (Table
862 S9). Remarkably, none of those abovementioned strains were isolated from Chinese
863 Spring infected plants.
864
865 For NA, *Pararheinheimera sp* (AF0141), *Pseudomonas hunanensis* (AF0142), *Baliella*
866 *marina* (AF0012*), Flavobacterium hydatis* (AF0027), *Microbacterium sp* (AF0077),
867 *Bacillus thuringiensis* (AF0154), and *Caulobacter sp* (AF0118) were the most
868 promoted strains, while *Acidovorax sp* (AF0089), *Curtobacterium flaccumfaciens*
869 (AF0165), *Variovorax beijingensis* (AF0128), *Curtobacterium oceanosedimentum*
870 (AF0004), *Kineococus sp* (AF0060), *Pseudomonas anguilliseptica* (AF0162),
871 *Rhizobium sp* (AF0164), and *Leifsonia shinshuensis* (AF0088) were the most inhibited
872 strains (Table S9). The microbes AF0141, AF0142, AF0154, AF0162, AF0164, and
873 AF0165 were isolated from *Z. tritici*-infected Chinese Spring plants, and we

874 hypothesized that *Pararheinheimera sp, Pseudomonas hunanensis,* and *Bacillus*
875 *thuringiensis* may benefit from the accumulation of nonanoic acid in the apoplast and
876 these microbes may potentially play a role in the plant-pathogen interaction. On the
877 other hand, *Pseudomonas anguilliseptica, Rhizobium sp*, and *Curtobacterium*
878 *flaccumfaciens* may be sensitive to the pathogen-induced immune response.
879
880 Finally, for QA, we observed that *Pseudomonas putida* (AF0171), *Pseudomonas*
881 *hunanensis* (AF0142), *Pararheinheimera sp* (AF0141), *Pseudomonas umsongensis*
882 (AF0144), *Chrysepbacterium taeanense* (AF0131), *Pseudomonas anguilliseptica*
883 (AF0138), *Acidovorax facilis* (AF0014), and *Pseudomonas rhodesiae* (AF0111 and
884 AF0139) were the most promoted strains, while *Pseudomonas sp* (AF0130),
885 *Agrobacterium tumefaciens* (AF0129), *Pseudomonas frederiksbergensis* (AF0191),
886 *Pseudomonas brassicacearum* (AF0029, AF0102, and AF0120), *Sphingobium*
887 *bisphenolicum* (AF0048), and *Microbacterium proteolyticum* (AF0059) were the most
888 inhibited strains (Table S9). The microbes AF0171, AF0138, AF0139, AF0141,
889 AF0142, AF0144, and AF0191 were isolated from *Z. tritici*-infected Chinese Spring
890 plants, and we hypothesized that different *Pseudomonas* and *Pararheinheimera*
891 species may benefit from the production of quinic acid during the induced defense
892 response. Contrarily, *Pseudomonas frederiksbergensis* appears to be sensitive to the
893 defense related compound.
894
895 In summary, *Pseudomonas hunanensis* (AF0141) and *Pararheinheimera sp* (AF0142)
896 were the two bacteria isolated from *Z. tritici*-infected Chinese Spring plants which
897 showed growth promotion when exposed to both NA and QA, while *Agrobacterium*
898 *tumefaciens* (AF0129), *Acidovorax sp* (AF0089), and *Pseudomonas brassicacearum*

899 (AF0120) isolated from the mock-treated Chinese Spring plants were the most
900 inhibited microbes (Table S9). The 10 most promoted and inhibited microbes over the
901 time course of the experiment are summarized in Table S9. These findings
902 demonstrate a remarkable variation in the tolerance of apoplast-associated microbes
903 to plant compounds previously shown to be induced during *Z. tritici* infection. Future
904 studies should address the molecular mechanism underlying the growth inhibition and
905 promotion and their impact for plant health and pathogenesis.
906
907 **DISCUSSSION**
908 In their natural environment, plants are constantly challenged by pathogenic
909 organisms which attempt to invade below and above ground tissues. Pathogenic
910 organisms can induce immune responses conferring significant alterations in the
911 composition of molecules which are secreted into the apoplastic space. In response,
912 plants produce and secrete a variety of antimicrobial proteins and metabolites to
913 hamper pathogen invasion. How do commensal microorganisms that inhabit the
914 apoplastic space cope with recurrent biotic stress responses? We addressed this
915 question in our study by characterizing fluctuations in biotic conditions in wheat
916 apoplast and by investigating specific adaptations of apoplast-associated microbes.
917
918 We successfully isolated apoplastic fluids from the two wheat genotypes, Obelisk and
919 Chinese Spring, allowing us to characterize the biochemical environment between
920 cells in the leaf mesophyll. The two wheat genotypes are genetically different; Obelisk
921 is an inbred cultivar while Chinese Spring is a landrace known to have a broader
922 resistance spectrum towards pathogens (78). In our comparative proteome analysis,
923 first of all, we observed a considerable differentiation in protein composition between

924 the two wheat genotypes. The different genetic-make up of these two wheat genotypes
925 may to some extent explain differences in proteome content; however, we cannot
926 exclude that the two genotypes also differ in the amenability of protein extraction.
927
928 Obelisk and Chinese Spring differ in their resistance towards the *Z. tritici* isolate
929 IPO323. This is due to the production of the cell wall associated immune receptor Stb6
930 in Chinese Spring; a receptor that is activated by the secreted protein AvrStb6 that is
931 produced by IPO323. We previously showed that the abundance of immune-related
932 metabolites is significantly up-regulated in Chinese Spring during early invasion of *Z.*
933 *tritici* (10). In contrast, the production of immune-related metabolites is suppressed in
934 Obelisk during IPO323 invasion. Proteome analyses of infected Obelisk and Chinese
935 Spring leaves showed a common response to fungal invasion, suggesting a conserved
936 initial response to fungal invasion (Fig. 1C). The ns-LPTs (containing bifunctional
937 inhibitor/plant lipid transfer protein/seed storage helical domain), for example, have
938 been implicated in the regulation of plant defense responses against various
939 pathogens (61). Additionally, peroxidases are upregulated in both wheat genotypes
940 during *Z. tritici* infection. Peroxidases are enzymes are known to play a crucial role in
941 the generation of reactive oxygen species, an initial defense response conferring
942 downstream immune signaling and local plant cell death (79, 80). Although Obelisk is
943 susceptible to the invasion of the *Z. tritici* isolate IPO323, we recognize several
944 defense related responses reflected in an upregulation of endochitinases, chitinases,
945 and a serine carboxypeptidase, each consistent with the activation of defenses against
946 fungal pathogens (81-83). Endochitinases and chitinases are enzymes involved in the
947 degradation of chitin, a component of fungal cell walls, while serine carboxypeptidases
948 have been implicated in the defense against fungal pathogens by cleavage off

949 essential amino acids from fungal cell walls. In contrast, proteins that are specifically
950 upregulated in Chinese Spring reflect a different mechanism of defense responses
951 (*e.g.,* defensins, thaumatin, aspartyl proteases, and GDSL esterase/lipase). Defensins
952 are small cysteine-rich peptides with antifungal activity, while thaumatin is known to
953 have antifungal and antibacterial properties (84-86). Aspartyl proteases play a role in
954 plant cell death and the degradation of invading pathogens, while GDSL
955 esterase/lipases are involved in the regulation of plant defense responses against
956 various pathogens (87, 88). We also observe an upregulation of ns-LTPs in Chinese
957 Spring, which may be an important component of the systemic acquired resistance
958 (SAR) induced by *Z. tritici* in the resistant cultivar (10). In *Arabidopsis*, the ns-LTPs are
959 induced by immune signaling and secreted into the apoplast where they participate in
960 the intercellular, long-distance transport of lipids, acting as crucial signaling molecules
961 in the induction and propagation of defense responses (89). This systemic lipid
962 transfer is believed to prime uninfected tissues, enabling a robust defense response
963 upon subsequent pathogen attack. Furthermore, ns-LTPs have been implicated in
964 enhancing the stability of lipid rafts in the plasma membrane, which act as signaling
965 platforms for immune receptors and downstream defense-related signaling molecules
966 (89, 90). In summary, the proteome data presented here provides an accurate and
967 novel catalogue of conserved and genotype specific apoplast proteins, including
968 shared and specific defense-related proteins. We specifically identify components of
969 systemic immune signaling in Chinese Spring, which may be considered in future
970 breeding strategies. Interestingly, *Z. tritici* appear to be tolerant to a variety of defense
971 related proteins which are upregulated in the susceptible Obelisk, but without effect
972 on pathogen propagation.
973

From the apoplasic fluid samples we also isolated endophytic bacteria and fungi. Such broader approach allowed us to characterize not only microbial diversity, but also the footprints of microbial adaptations to varying wheat defense responses. Importantly, our studied was designed in a way that the two wheat genotypes were grown in the same soil and thereby provided with the same source of microbial communities. We recognize that the culture-based approach allows us to characterize only a subset of the complete microbiota diversity. Thereby, we can neither make conclusive statements about differences between wheat genotypes or conditions as the sampling efficacy may be biased by our ability to isolate and cultivate specific microbes. In total we isolate 667 microbes comprising 59 different taxa. In our study, we observed that the wheat-recovered microbes were predominantly composed of Gammaproteobacteria within the Proteobacteria phylum. This result is consistent with previous studies reporting the enrichment of Gammaproteobacterial class in various wheat genotypes and plant compartments (91-93). However, we identified a clear and significant shift from Proteobacteria to Actinobacteria specifically during the compatible interaction, where Obelisk wheat was infected by *Zymoseptoria tritici*. This shift suggests that the defense responses elicited by Obelisk may have a detrimental effect on Proteobacteria endophytes. The transition from Proteobacteria to Actinobacteria can have profound implications for the ecosystem's functioning and plant health. The capacity of Actinobacteria to degrade complex organic compounds, such as cellulose and lignin, can influence nutrient cycling and organic matter decomposition, thereby impacting ecosystem processes. Proteobacteria, particularly Alpha- and Gamma-Proteobacteria, contribute to plant growth promotion, nitrogen fixation, and biocontrol activities, while Actinobacteria are known to assist in plant defense against pathogens (94, 95). Consequently, a shift from Proteobacteria to

999 Actinobacteria may disrupt these beneficial interactions, potentially compromising
1000 plant growth, disease resistance, and overall plant health. Furthermore, this shift could
1001 lead to reduced functional redundancy and decreased resilience within the microbial
1002 community, rendering it more susceptible to environmental disturbances. Additionally,
1003 alterations in microbial interactions can occur, influencing the dynamics of the entire
1004 microbial community. To comprehensively understand the consequences of the
1005 Proteobacteria to Actinobacteria shift, context-specific studies are needed to unravel
1006 its effects on ecosystem processes and plant-microbe interactions.
1007
1008 In terms of microbiota disappearance and resilience, we unveiled that *Pseudomonas*
1009 were eliminated during the compatible interaction, while *Curtobacterium* and
1010 *Sphingomonas* were the only two genera resilient to defense responses of the
1011 susceptible Obelisk. In fact, we observed that *Curtobacterium* and *Sphingomonas*
1012 species were highly tolerant when challenged against exogenous H_2O_2 in our *in vitro*
1013 assays. These findings are in agreement with a previous study that demonstrated
1014 extensive ROS production *in planta* in a susceptible interaction (96). ROS, generated
1015 by plants as defense mechanisms against pathogens and environmental stresses, can
1016 significantly influence the colonization and behavior of endophytes. Elevated ROS
1017 levels may impede endophytic colonization or induce alterations in microbial gene
1018 expression and metabolic pathways. Nevertheless, certain endophytic microbes have
1019 evolved mechanisms to tolerate or exploit ROS as signaling molecules (73). Thus, we
1020 postulated that the Obelisk-infected associated microbes were more resilient to H_2O_2
1021 due to their previous adaptation to cope with oxidative stress generated during wheat
1022 development and/or abiotic/biotic stress. Regarding *Pseudomonas*, we observed *in*
1023 *vitro* that this bacterial genus, overall, show a lower tolerance to exogenous H_2O_2.

1024 *Pseudomonas* was also the dominant genus recovered from the incompatible
1025 interaction. A previous study showed that in an incompatible interaction of Stb6-
1026 AvrStb6 free radicals such H_2O_2 are neutralized at the biotrophic phase, preventing
1027 the oxidative burst (24). Therefore, we hypothesized that the lower concentration of
1028 apoplastic H_2O_2 in the incompatible interaction enabled *Pseudomonas* species to
1029 colonize the apoplastic space of the resistant Chinese Spring plants. However, when
1030 evaluating *Pseudomonas* species against three exogenous wheat secondary
1031 metabolites, we observed that this bacterial genus displayed the highest tolerance
1032 levels among all microbial species. These three secondary metabolites were
1033 previously found to be enriched *in planta* during the wheat incompatible interaction
1034 (10). Plant-produced secondary metabolites, including phytochemicals and
1035 antimicrobial compounds, can impact endophytic microbial communities by either
1036 inhibiting or stimulating their growth and activity. We then hypothesized that the
1037 predominance of *Pseudomonas* genus in Chinese Spring plants is due to the reduced
1038 H_2O_2 and higher tolerance to secondary metabolites in the apoplast space. These
1039 reciprocal interactions among ROS, secondary metabolites, and endophytic microbes
1040 constitute a complex and dynamic relationship that profoundly shapes the composition
1041 and functionality of the endophytic microbiome. Another evidence of this complexity is
1042 reflected in the high potential of *Pseudomonas* species to inhibit *Z. tritici* growth *in*
1043 *vitro*, while this bacterial genus is depleted in the compatible interaction.
1044
1045 Our findings provide novel evidence for the impact of *Z. tritici* on defense responses
1046 and physiological processes in the infected plant tissue. We provided evidences that
1047 specific components of plant-immune responses shape microbial profiles leading to
1048 the prevalence of microbes adapted to oxidative stress or secondary metabolites,

depending on the outcome of the host-pathogen interaction responses. Further studies will be necessary to address the impact of the apparent shift in dominance from Proteobacteria to Actinobacteria in the susceptible Obelisk, as well as the direct endophytic-triggered inhibition of *Z. tritici* growth during plant colonization and the onset of disease.

Data availability:

Proteome data is made available upon request.

Wheat-associated microbes are stored at -80C in the lab of EHS, CAU Kiel and are available upon request.

Author contributions:

Conceptualization: CSF, EHS

Methodology: CSF, MA, LC, MH

Formal analyses and investigation: CSF, MA, CI, and JG

Resources: EHS and AT

Writing of original draft: CSF, EHS

Review and editing: All authors

Funding acquisition: EHS, AT

Acknowledgements:

This research was funded by the German Research Foundation in the framework of the collaborative research center “Origin and Function of Metaorganisms”, CRC1182, sub-project A3 and Z3. We thank Dr. Danilo A. dos Santos Pereira and Dr. Marco

Alexandre Guerreiro for sharing R scripts. We also thank Susanne Braun for the remarkable technical support.

References

1. Muller DB, Vogel C, Bai Y, Vorholt JA. 2016. The Plant Microbiota: Systems-Level Insights and Perspectives. Annu Rev Genet 50:211-234.
2. Hassani MA, Ozkurt E, Seybold H, Dagan T, Stukenbrock EH. 2019. Interactions and Coadaptation in Plant Metaorganisms. Annu Rev Phytopathol 57:483-503.
3. Trivedi P, Leach JE, Tringe SG, Sa T, Singh BK. 2020. Plant-microbiome interactions: from community assembly to plant health. Nat Rev Microbiol 18:607-621.
4. Turner TR, James FK, Poole PS. 2013. The plant microbiome. Genome Biology 14.
5. Hardoim PR, van Overbeek LS, Berg G, Pirttila AM, Compant S, Campisano A, Doring M, Sessitsch A. 2015. The Hidden World within Plants: Ecological and Evolutionary Considerations for Defining Functioning of Microbial Endophytes. Microbiol Mol Biol Rev 79:293-320.
6. Bodenhausen N, Bortfeld-Miller M, Ackermann M, Vorholt JA. 2014. A synthetic community approach reveals plant genotypes affecting the phyllosphere microbiota. PLoS Genet 10:e1004283.
7. Muller DB, Schubert OT, Rost H, Aebersold R, Vorholt JA. 2016. Systems-level Proteomics of Two Ubiquitous Leaf Commensals Reveals Complementary Adaptive Traits for Phyllosphere Colonization. Mol Cell Proteomics 15:3256-3269.
8. Lebeis SL, Paredes SH, Lundberg DS, Breakfield N, Gehring J, McDonald M, Malfatti S, Del Rio TG, Jones CD, Tringe SG, Dangl JL. 2015. Salicylic acid modulates colonization of the root microbiome by specific bacterial taxa. Science 349:860 - 864.
9. Pfeilmeier S, Petti GC, Bortfeld-Miller M, Daniel B, Field CM, Sunagawa S, Vorholt JA. 2021. The plant NADPH oxidase RBOHD is required for microbiota homeostasis in leaves. Nat Microbiol 6:852-864.
10. Seybold H, Demetrowitsch TJ, Hassani MA, Szymczak S, Reim E, Haueisen J, Lubbers L, Ruhlemann M, Franke A, Schwarz K, Stukenbrock EH. 2020. A fungal pathogen induces systemic susceptibility and systemic shifts in wheat metabolome and microbiome composition. Nat Commun 11:1910.
11. Couto D, Zipfel C. 2016. Regulation of pattern recognition receptor signalling in plants. Nat Rev Immunol 16:537-52.
12. Bjornson M, Pimprikar P, Nurnberger T, Zipfel C. 2021. The transcriptional landscape of Arabidopsis thaliana pattern-triggered immunity. Nat Plants 7:579-586.
13. Fan L, Frohlich K, Melzer E, Pruitt RN, Albert I, Zhang L, Joe A, Hua C, Song Y, Albert M, Kim ST, Weigel D, Zipfel C, Chae E, Gust AA, Nurnberger T. 2022. Genotyping-by-sequencing-based identification of Arabidopsis pattern recognition receptor RLP32 recognizing proteobacterial translation initiation factor IF1. Nat Commun 13:1294.
14. Latz MAC, Kerrn MH, Sorensen H, Collinge DB, Jensen B, Brown JKM, Madsen AM, Jorgensen HJL. 2021. Succession of the fungal endophytic microbiome of wheat is dependent on tissue-specific interactions between host genotype and environment. Sci Total Environ 759:143804.

1116 15. Rojas EC, Jensen B, Jørgensen HJL, Latz MAC, Esteban P, Ding Y, Collinge DB. 2020.
1117 Selection of fungal endophytes with biocontrol potential against Fusarium head
1118 blight in wheat. Biological Control 144.
1119 16. Hone H, Mann R, Yang G, Kaur J, Tannenbaum I, Li T, Spangenberg G, Sawbridge T.
1120 2021. Profiling, isolation and characterisation of beneficial microbes from the seed
1121 microbiomes of drought tolerant wheat. Sci Rep 11:11916.
1122 17. Zhong Z, Marcel TC, Hartmann FE, Ma X, Plissonneau C, Zala M, Ducasse A, Confais J,
1123 Compain J, Lapalu N, Amselem J, McDonald BA, Croll D, Palma-Guerrero J. 2017. A
1124 small secreted protein in Zymoseptoria tritici is responsible for avirulence on wheat
1125 cultivars carrying the Stb6 resistance gene. New Phytol 214:619-631.
1126 18. Karlstedt F, Kopahnke D, Perovic D, Jacobi A, Pillen K, Ordon F. 2019. Mapping of
1127 quantitative trait loci (QTL) for resistance against Zymoseptoria tritici in the winter
1128 spelt wheat accession HTRI1410 (Triticum aestivum subsp. spelta). Euphytica 215.
1129 19. Mahboubi M, Talebi R, Mehrabi R, Mohammad Naji A, Maccaferri M, Kema GHJ.
1130 2022. Genetic analysis of novel resistance sources and genome-wide association
1131 mapping identified novel QTLs for resistance to Zymoseptoria tritici, the causal agent
1132 of septoria tritici blotch in wheat. J Appl Genet 63:429-445.
1133 20. Yang N, Ovenden B, Baxter B, McDonald MC, Solomon PS, Milgate A. 2022. Multi-
1134 stage resistance to Zymoseptoria tritici revealed by GWAS in an Australian bread
1135 wheat diversity panel. Front Plant Sci 13:990915.
1136 21. Amezrou R, Audeon C, Compain J, Gelisse S, Ducasse A, Saintenac C, Lapalu N, Louet
1137 C, Orford S, Croll D, Amselem J, Fillinger S, Marcel TC. 2023. A secreted protease-like
1138 protein in Zymoseptoria tritici is responsible for avirulence on Stb9 resistance gene
1139 in wheat. PLoS Pathog 19:e1011376.
1140 22. Kema GHJ, Mirzadi Gohari A, Aouini L, Gibriel HAY, Ware SB, van den Bosch F,
1141 Manning-Smith R, Alonso-Chavez V, Helps J, Ben M'Barek S, Mehrabi R, Diaz-Trujillo
1142 C, Zamani E, Schouten HJ, van der Lee TAJ, Waalwijk C, de Waard MA, de Wit P,
1143 Verstappen ECP, Thomma B, Meijer HJG, Seidl MF. 2018. Stress and sexual
1144 reproduction affect the dynamics of the wheat pathogen effector AvrStb6 and
1145 strobilurin resistance. Nat Genet 50:375-380.
1146 23. Saintenac C, Lee WS, Cambon F, Rudd JJ, King RC, Marande W, Powers SJ, Berges H,
1147 Phillips AL, Uauy C, Hammond-Kosack KE, Langin T, Kanyuka K. 2018. Wheat
1148 receptor-kinase-like protein Stb6 controls gene-for-gene resistance to fungal
1149 pathogen Zymoseptoria tritici. Nat Genet 50:368-374.
1150 24. Ghiasi Noei F, Imami M, Didaran F, Ghanbari MA, Zamani E, Ebrahimi A, Aliniaeifard
1151 S, Farzaneh M, Javan-Nikkhah M, Feechan A, Mirzadi Gohari A. 2022. Stb6 mediates
1152 stomatal immunity, photosynthetic functionality, and the antioxidant system during
1153 the Zymoseptoria tritici-wheat interaction. Front Plant Sci 13:1004691.
1154 25. Kema GHJ, Cor HVS. 1997. Genetic Variation for Virulence and Resistancein the
1155 Wheat-Mycosphaerella graminicola PathosystemIII. Comparative Seedling and Adult
1156 Plant Experiments. Phytopathology 87:266-272.
1157 26. Thygesen K, Jørgensen LN, Jensen KS, Munk L. 2008. Spatial and temporal impact of
1158 fungicide spray strategies on fungicide sensitivity of Mycosphaerella graminicola in
1159 winter wheat. European Journal of Plant Pathology 123:435-447.
1160 27. Stukenbrock EH, Banke S, Javan-Nikkhah M, McDonald BA. 2007. Origin and
1161 domestication of the fungal wheat pathogen Mycosphaerella graminicola via
1162 sympatric speciation. Mol Biol Evol 24:398-411.

1163 28. Francisco CS, Zwyssig MM, Palma-Guerrero J. 2020. The role of vegetative cell
1164 fusions in the lifestyle of the wheat fungal pathogen *Zymoseptoria tritici*. bioRxiv
1165 doi:10.1101/2020.01.26.918797.
1166 29. Nakano RT, Ishihama N, Wang Y, Takagi J, Uemura T, Schulze-Lefert P, Nakagami H.
1167 2020. Apoplastic Fluid Preparation from Arabidopsis thaliana Leaves Upon
1168 Interaction with a Nonadapted Powdery Mildew Pathogen. *In* J. J-N, L. V, M. C, Rey
1169 MD (ed), Plant Proteomics Methods in Molecular Biology, vol 2139. Humana, New
1170 York.
1171 30. Tyanova S, Temu T, Sinitcyn P, Carlson A, Hein MY, Geiger T, Mann M, Cox J. 2016.
1172 The Perseus computational platform for comprehensive analysis of (prote)omics
1173 data. Nat Methods 13:731-40.
1174 31. Bedre R. 2020. eneshbedre/bioinfokit: Bioinformatics data analysis and visualization
1175 toolkit. Zenodo doi:http://doi.org/10.5281/zenodo.3698145.
1176 32. Sherman BT, Hao M, Qiu J, Jiao X, Baseler MW, Lane HC, Imamichi T, Chang W. 2022.
1177 DAVID: a web server for functional enrichment analysis and functional annotation of
1178 gene lists (2021 update). Nucleic Acids Res 50:W216-21.
1179 33. Huang da W, Sherman BT, Lempicki RA. 2009. Systematic and integrative analysis of
1180 large gene lists using DAVID bioinformatics resources. Nat Protoc 4:44-57.
1181 34. Sperschneider J, Dodds PN, Singh KB, Taylor JM. 2018. ApoplastP: prediction of
1182 effectors and plant proteins in the apoplast using machine learning. New Phytol
1183 217:1764-1778.
1184 35. Teufel F, Almagro Armenteros JJ, Johansen AR, Gislason MH, Pihl SI, Tsirigos KD,
1185 Winther O, Brunak S, von Heijne G, Nielsen H. 2022. SignalP 6.0 predicts all five types
1186 of signal peptides using protein language models. Nat Biotechnol 40:1023-1025.
1187 36. Oliveros JC. 2007-2015. Venny. An interactive tool comparing lists with Venn's
1188 diagrams.
1189 37. Marchesi JR, Sato T, Weightman AJ, Martin TA, Fry JC, Hiom SJ, Wade WG. 1998.
1190 Design and Evaluation of Useful Bacterium-Specific PCR Primers That Amplify Genes
1191 Coding for Bacterial 16S rRNA. Applied and Environmental Microbiology 64:795-799.
1192 38. Bellemain E, Casrlsen T, Brochmann C, Coissac E, Taberlet P, Kauserud H. 2010. ITS as
1193 an environmental DNA barcode for fungi- an in silico approach reveals potential PCR
1194 biases. BMC Microbiology 10:1-9.
1195 39. Pruesse E, Peplies J, Glockner FO. 2012. SINA: accurate high-throughput multiple
1196 sequence alignment of ribosomal RNA genes. Bioinformatics 28:1823-9.
1197 40. Tamura K, Stecher G, Kumar S. 2021. MEGA11: Molecular Evolutionary Genetics
1198 Analysis Version 11. Mol Biol Evol 38:3022-3027.
1199 41. Stamatakis A. 2014. RAxML version 8: a tool for phylogenetic analysis and post-
1200 analysis of large phylogenies. Bioinformatics 30:1312-3.
1201 42. Anderson MJ, Crist TO, Chase JM, Vellend M, Inouye BD, Freestone AL, Sanders NJ,
1202 Cornell HV, Comita LS, Davies KF, Harrison SP, Kraft NJ, Stegen JC, Swenson NG.
1203 2011. Navigating the multiple meanings of beta diversity: a roadmap for the
1204 practicing ecologist. Ecol Lett 14:19-28.
1205 43. Larkin MA, Blackshields G, Brown NP, Chenna R, McGettigan PA, McWilliam H,
1206 Valentin F, Wallace IM, Wilm A, Lopez R, Thompson JD, Gibson TJ, Higgins DG. 2007.
1207 Clustal W and Clustal X version 2.0. Bioinformatics 23:2947-8.
1208 44. Dhar A, Minin VN. 2016. Maximum Likelihood Phylogenetic Inference, p 499-506,
1209 Encyclopedia of Evolutionary Biology doi:10.1016/b978-0-12-800049-6.00207-9.

1210 45. Letunic I, Bork P. 2021. Interactive Tree Of Life (iTOL) v5: an online tool for
1211 phylogenetic tree display and annotation. Nucleic Acids Res 49:W293-W296.
1212 46. Haueisen J, Moller M, Eschenbrenner CJ, Grandaubert J, Seybold H, Adamiak H,
1213 Stukenbrock EH. 2019. Highly flexible infection programs in a specialized wheat
1214 pathogen. Ecol Evol 9:275-294.
1215 47. Schneider CA, Rasband WS, Eliceiri KW. 2012. NIH Image to ImageJ: 25 years of
1216 image analysis. Nature Methods 9:671.
1217 48. Nishad R, Ahmed T, Rahman VJ, Kareem A. 2020. Modulation of Plant Defense
1218 System in Response to Microbial Interactions. Front Microbiol 11:1298.
1219 49. Seybold H, Demetrowitsch T, Hassani MA, Szymczak S, Reim E, Haueisen J,
1220 Rühlemann M, Franke A, Schwarz K, Stukenbrock EH. 2019. Hemibiotrophic fungal
1221 pathogen induces systemic susceptibility and systemic shifts in wheat metabolome
1222 and microbiome composition. bioRxiv doi:10.1101/702373.
1223 50. Wickham H. 2009. ggplot2: Elegant Graphics for Data Analysis. Use R. Springer-
1224 Verlag, New York.
1225 51. Chartrain L, Brading PA, Brown JKM. 2005. Presence of the Stb6 gene for resistance
1226 to septoria tritici blotch (Mycosphaerella graminicola) in cultivars used in wheat-
1227 breeding programmes worldwide. Plant Pathology 54:134-143.
1228 52. Palma-Guerrero J, Ma X, Torriani SF, Zala M, Francisco CS, Hartmann FE, Croll D,
1229 McDonald BA. 2017. Comparative Transcriptome Analyses in Zymoseptoria tritici
1230 Reveal Significant Differences in Gene Expression Among Strains During Plant
1231 Infection. Mol Plant Microbe Interact 30:231-244.
1232 53. Mamaeva A, Taliansky M, Filippova A, Love AJ, Golub N, Fesenko I. 2020. The role of
1233 chloroplast protein remodeling in stress responses and shaping of the plant
1234 peptidome. New Phytol 227:1326-1334.
1235 54. Zhou Y, Wang B, Yuan F. 2022. The Role of Transmembrane Proteins in Plant Growth,
1236 Development, and Stress Responses. Int J Mol Sci 23.
1237 55. Xiong W, Lan T, Mo B. 2021. Extraribosomal Functions of Cytosolic Ribosomal
1238 Proteins in Plants. Front Plant Sci 12:607157.
1239 56. Hussain A, Asif N, Pirzada AR, Noureen A, Shaukat J, Burhan A, Zaynab M, Ali E, Imran
1240 K, Ameen A, Mahmood MA, Nazar A, Mukhtar MS. 2022. Genome wide study of
1241 cysteine rich receptor like proteins in Gossypium sp. Sci Rep 12:4885.
1242 57. Vaattovaara A, Brandt B, Rajaraman S, Safronov O, Veidenberg A, Luklová M,
1243 Kangasjärvi J, Löytynoja A, Hothorn M, Salojärvi J, Wrzaczek M. 2019. Mechanistic
1244 insights into the evolution of DUF26-containing proteins in land plants.
1245 Communications Biology 2.
1246 58. de Lorenzo G, D''Ovidio R, Cervone F. 2001. The role of polygalacturonase-inhibiting
1247 proteins (PGIPs) in defense against poathogenic fungi. Annual Review of
1248 Phytopathology 39:313-315.
1249 59. Wei W, Xu L, Peng H, Zhu W, Tanaka K, Cheng J, Sanguinet KA, Vandemark G, Chen
1250 W. 2022. A fungal extracellular effector inactivates plant polygalacturonase-
1251 inhibiting protein. Nat Commun 13:2213.
1252 60. Federici L, Di Matteo A, Fernandez-Recio J, Tsernoglou D, Cervone F. 2006.
1253 Polygalacturonase inhibiting proteins: players in plant innate immunity? Trends Plant
1254 Sci 11:65-70.

1255 61. Gao H, Ma K, Ji G, Pan L, Zhou Q. 2022. Lipid transfer proteins involved in plant-
1256 pathogen interactions and their molecular mechanisms. Mol Plant Pathol 23:1815-
1257 1829.
1258 62. Soprano AS, Smetana JHC, Benedetti CE. 2018. Regulation of tRNA biogenesis in
1259 plants and its link to plant growth and response to pathogens. Biochim Biophys Acta
1260 Gene Regul Mech 1861:344-353.
1261 63. Moeller JR, Moscou MJ, Bancroft T, Skadsen RW, Wise RP, Whitham SA. 2012.
1262 Differential accumulation of host mRNAs on polyribosomes during obligate
1263 pathogen-plant interactions. Mol Biosyst 8:2153-65.
1264 64. Camborde L, Kiselev A, Pel MJC, Le Ru A, Jauneau A, Pouzet C, Dumas B, Gaulin E.
1265 2022. An oomycete effector targets a plant RNA helicase involved in root
1266 development and defense. New Phytol 233:2232-2248.
1267 65. Ahn CS, Cho HK, Lee DH, Sim HJ, Kim SG, Pai HS. 2016. Functional characterization of
1268 the ribosome biogenesis factors PES, BOP1, and WDR12 (PeBoW), and mechanisms
1269 of defective cell growth and proliferation caused by PeBoW deficiency in
1270 Arabidopsis. J Exp Bot 67:5217-32.
1271 66. Ramesh P, Bajire SK, Kanichery A, Najar MA, Shastry RP, Prasad TSK. 2022. 6-
1272 Methylcoumarin rescues bacterial quorum sensing induced ribosome-inactivating
1273 stress in Caenorhabditis elegans. Microb Pathog 173:105833.
1274 67. Rudd JJ, Kanyuka K, Hassani-Pak K, Derbyshire M, Andongabo A, Devonshire J,
1275 Lysenko A, Saqi M, Desai NM, Powers SJ, Hooper J, Ambroso L, Bharti A, Farmer A,
1276 Hammond-Kosack KE, Dietrich RA, Courbot M. 2015. Transcriptome and metabolite
1277 profiling of the infection cycle of Zymoseptoria tritici on wheat reveals a biphasic
1278 interaction with plant immunity involving differential pathogen chromosomal
1279 contributions and a variation on the hemibiotrophic lifestyle definition. Plant Physiol
1280 167:1158-85.
1281 68. Sperschneider J, Dodds PN. 2022. EffectorP 3.0: Prediction of Apoplastic and
1282 Cytoplasmic Effectors in Fungi and Oomycetes. Mol Plant Microbe Interact 35:146-
1283 156.
1284 69. Lee SM, Kong HG, Song GC, Ryu CM. 2021. Disruption of Firmicutes and
1285 Actinobacteria abundance in tomato rhizosphere causes the incidence of bacterial
1286 wilt disease. ISME J 15:330-347.
1287 70. Snelders NC, Boshoven JC, Song Y, Schmitz N, Fiorin GL, Rovenich H, van den Berg
1288 GCM, Torres DE, Petti GC, Prockl Z, Faino L, Seidl MF, Thomma B. 2023. A highly
1289 polymorphic effector protein promotes fungal virulence through suppression of
1290 plant-associated Actinobacteria. New Phytol 237:944-958.
1291 71. Carlstrom CI, Field CM, Bortfeld-Miller M, Muller B, Sunagawa S, Vorholt JA. 2019.
1292 Synthetic microbiota reveal priority effects and keystone strains in the Arabidopsis
1293 phyllosphere. Nat Ecol Evol 3:1445-1454.
1294 72. Gómez-Pérez D, Schmid M, Chaudhry V, Velic A, Maček B, Kemen A, Kemen E. 2022.
1295 Proteins released into the plant apoplast by the obligate parasitic protist Albugo
1296 selectively repress phyllosphere-associated bacteria. bioRxiv
1297 doi:10.1101/2022.05.16.492175.
1298 73. Sahu PK, Jayalakshmi K, Tilgam J, Gupta A, Nagaraju Y, Kumar A, Hamid S, Singh HV,
1299 Minkina T, Rajput VD, Rajawat MVS. 2022. ROS generated from biotic stress: Effects
1300 on plants and alleviation by endophytic microbes. Front Plant Sci 13:1042936.

1301 74. Zhong Z, McDonald BA, Palma-Guerrero J. 2021. Tolerance to oxidative stress is
1302 associated with both oxidative stress response and inherent growth in a fungal
1303 wheat pathogen. Genetics 217.
1304 75. Hashem A, Alqarawi AA, Radhakrishnan R, Al-Arjani AF, Aldehaish HA, Egamberdieva
1305 D, Abd Allah EF. 2018. Arbuscular mycorrhizal fungi regulate the oxidative system,
1306 hormones and ionic equilibrium to trigger salt stress tolerance in Cucumis sativus L.
1307 Saudi J Biol Sci 25:1102-1114.
1308 76. Fountain JC, Bajaj P, Nayak SN, Yang L, Pandey MK, Kumar V, Jayale AS, Chitikineni A,
1309 Lee RD, Kemerait RC, Varshney RK, Guo B. 2016. Responses of Aspergillus flavus to
1310 Oxidative Stress Are Related to Fungal Development Regulator, Antioxidant Enzyme,
1311 and Secondary Metabolite Biosynthetic Gene Expression. Front Microbiol 7:2048.
1312 77. Singh Y, Nair AM, Verma PK. 2021. Surviving the odds: From perception to survival of
1313 fungal phytopathogens under host-generated oxidative burst. Plant Commun
1314 2:100142.
1315 78. International Wheat Genome Sequencing C. 2018. Shifting the limits in wheat
1316 research and breeding using a fully annotated reference genome. Science 361.
1317 79. Daudi A, Cheng Z, O'Brien JA, Mammarella N, Khan S, Ausubel FM, Bolwell GP. 2012.
1318 The apoplastic oxidative burst peroxidase in Arabidopsis is a major component of
1319 pattern-triggered immunity. Plant Cell 24:275-87.
1320 80. Tripathy BC, Oelmuller R. 2012. Reactive oxygen species generation and signaling in
1321 plants. Plant Signal Behav 7:1621-33.
1322 81. Burchacka E, Pieta P, Lupicka-Slowik A. 2022. Recent advances in fungal serine
1323 protease inhibitors. Biomed Pharmacother 146:112523.
1324 82. Fraser CM, Rider LW, Chapple C. 2005. An expression and bioinformatics analysis of
1325 the Arabidopsis serine carboxypeptidase-like gene family. Plant Physiol 138:1136-48.
1326 83. Bishop JG, Dean AM, Mitchell-Olds T. 200. Rapid evolution in plant chitinases:
1327 Molecular targets of selection in plant-pathogen coevolution. PNAS 97:5322-5327.
1328 84. Jiao W, Li X, Zhao H, Cao J, Jiang W. 2018. Antifungal Activity of an Abundant
1329 Thaumatin-Like Protein from Banana against Penicillium expansum, and Its Possible
1330 Mechanisms of Action. Molecules 23.
1331 85. Misra RC, Sandeep, Kamthan M, Kumar S, Ghosh S. 2016. A thaumatin-like protein of
1332 Ocimum basilicum confers tolerance to fungal pathogen and abiotic stress in
1333 transgenic Arabidopsis. Sci Rep 6:25340.
1334 86. Gorjanović S, Beljanski MV, Gavrović-Jankulović M, Gojgić-Cvijović G, Pavlović MD,
1335 Bejosano F. 2007. Antimicrobial Activity of Malting Barley Grain Thaumatin-Like
1336 Protein Isoforms, S and R. Journal of the Institute of Brewing 113:206-212.
1337 87. Gao M, Yin X, Yang W, Lam SM, Tong X, Liu J, Wang X, Li Q, Shui G, He Z. 2017. GDSL
1338 lipases modulate immunity through lipid homeostasis in rice. PLoS Pathog
1339 13:e1006724.
1340 88. Shen G, Sun W, Chen Z, Shi L, Hong J, Shi J. 2022. Plant GDSL Esterases/Lipases:
1341 Evolutionary, Physiological and Molecular Functions in Plant Development. Plants
1342 (Basel) 11.
1343 89. Maldonado AM, Doerner P, Dixon RA, Lamb CJ, Cameron RK. 2002. A putative lipid
1344 transfer protein involved in systemic resistance signalling in Arabidopsis. Nature
1345 419:399-403.

1346 90. Wang C, Gao H, Chu Z, Ji C, Xu Y, Cao W, Zhou S, Song Y, Liu H, Zhu C. 2021. A
1347 nonspecific lipid transfer protein, StLTP10, mediates resistance to Phytophthora
1348 infestans in potato. Mol Plant Pathol 22:48-63.
1349 91. Hassani MA, Özkurt E, Franzenburg S, Stukenbrock EH. 2020. Ecological Assembly
1350 Processes of the Bacterial and Fungal Microbiota of Wild and Domesticated Wheat
1351 Species. Phytobiomes Journal 4:217-224.
1352 92. Ozkurt E, Hassani MA, Sesiz U, Kunzel S, Dagan T, Ozkan H, Stukenbrock EH. 2020.
1353 Seed-Derived Microbial Colonization of Wild Emmer and Domesticated Bread Wheat
1354 (Triticum dicoccoides and T. aestivum) Seedlings Shows Pronounced Differences in
1355 Overall Diversity and Composition. mBio 11.
1356 93. Chen J, Sharifi R, Khan MSS, Islam F, Bhat JA, Kui L, Majeed A. 2021. Wheat
1357 Microbiome: Structure, Dynamics, and Role in Improving Performance Under Stress
1358 Environments. Front Microbiol 12:821546.
1359 94. Boukhatem ZF, Merabet C, Tsaki H. 2022. Plant Growth Promoting Actinobacteria,
1360 the Most Promising Candidates as Bioinoculants? Frontiers in Agronomy 4.
1361 95. Conn VM, Walker AR, Franco CMM. 2008. Endophytic Actinobacteria Induce Defense
1362 Pathways in Arabidopsis thaliana. Molecular Plant-Microbe Interactions 21:208-218.
1363 96. Shetty NP, Mehrabi R, Lutken H, Haldrup A, Kema GH, Collinge DB, Jorgensen HJ.
1364 2007. Role of hydrogen peroxide during the interaction between the hemibiotrophic
1365 fungal pathogen Septoria tritici and wheat. New Phytol 174:637-47.
1366

1367 **Figure legend**

1368

1369 **Figure 1. Proteomic analysis to study the impact of the *Zymoseptoria tritici* on**
1370 **the apoplastic proteome of the susceptible and resistant wheat genotypes.** (A)
1371 Scheme showing the quantitative proteomics used in this study. The pie chart
1372 demonstrated the 2'455 total proteins identified in the wheat apoplastic fluids. (B)
1373 Principal component analysis (PCA) of apoplastic proteomes of mock-treated and
1374 infected Obelisk and Chinese Spring plants. (C) Venn diagrams of 673 differentially
1375 expressed proteins in response to *Z. tritici* infection and shared between groups. In
1376 highlight, the 24 upregulated proteins exclusively found in Obelisk and Chinese Spring
1377 infected plants. (D) Volcano plot of differentially expressed proteins in the susceptible
1378 Obelisk. Light orange points represented the 242 proteins that were up-regulated in
1379 Obelisk infected plants (adjusted p-value <0.01; FC >2). The dark orange points
1380 represented the 299 proteins that were down-regulated in Obelisk during fungal

1381 infection (adjusted p-value <0.01; FC >2). (E) Volcano plot of differentially expressed
1382 proteins in the susceptible Chinese Spring. Light green points represented the 86
1383 proteins that were up-regulated in Chinese Spring infected plants (adjusted p-value
1384 <0.01; FC >2). The dark green points represented the 46 proteins that were down-
1385 regulated in Chinese Spring during fungal infection (adjusted p-value <0.01; FC >2).
1386 (F) Gene ontology (GO) enrichment terms for down-regulated (dark orange) and up-
1387 regulated (light orange) proteins in the susceptible Obelisk plants during fungal
1388 infection, respectively. (G) Gene ontology (GO) enrichment terms for down-regulated
1389 (dark green) and up-regulated (light green) proteins in the resistant Chinese Spring
1390 plants during fungal infection, respectively.
1391
1392 **Figure 2. Wheat-enriched endophytic community-based culture.** (A) Scheme
1393 showing the microbial isolation procedure used in this study. The pie chart
1394 demonstrated the 667 microbes isolated from the wheat apoplastic fluids, and the
1395 respective number of isolates per groups (mock-treated or infected Obelisk and
1396 Chinese Spring). (B) Wheat-enriched endophytic community-based culture collection
1397 is composed of 188 purified and archived isolates which were classified taxonomically
1398 using partial 16S rRNA and ITS sequences. These 188 microbes represent 59
1399 species. Venn diagrams showing the number of shared OTUs between groups. (C)
1400 Heatmap showing Jaccard index to compare the dissimilarity between microbial
1401 communities based on their species richness. (D) A reference phylogenetic tress of
1402 59 microbial species used in this study. Bar colors represent the corresponding phyla
1403 in all figures in this study. Black star indicates the ancestral of each phylum. Circles
1404 and squares represent the wheat genotypes and treatment from where the microbes
1405 were isolated. Dark or light orange circles indicated the microbe isolated from mock-

1406 treated or *Z. tritic*i infected Obelisk plants, respectively. Dark or light green squares
1407 indicated the microbe isolated from mock-treated or *Z. tritic*i infected Chinese Spring
1408 plants, respectively.
1409
1410 **Figure 3. The apoplast of wheat plants harbor an arsenal of potential**
1411 **antagonistic endophytes against *Zymoseptoria tritici*.** (A-B) Scheme and
1412 exemplification of the antagonistic assay performed *in vitro.* Plates containing solely
1413 Fries 3 medium were used as control to ensure microbial growth. Hygromycin B was
1414 used as positive control for fungal growth. (C) Three *Z. tritici* isolates were used in this
1415 study, such as the Dutch isolate IPO323, the Danish Zt05, and the Iranian Zt10.
1416 Roughly 20% of the wheat-recovered microbes were able to inhibited at least one of
1417 the *Z. tritici* isolates. Black points represent antagonistic microbes. Isolated that did
1418 not inhibited *Z. tritici* were excluded. The size of inhibition zones did not differ among
1419 the three tested *Z. tritici* isolates based on the Kruskal-Wallis statical analysis. (D)
1420 Proportion of microbes isolated from different wheat genotypes varying in the inhibitory
1421 activity against *Z. tritici*. (E) Composition of the wheat-enriched endophytic community-
1422 based culture (left) and the microbes inhibiting the three different *Z. tritici* isolates
1423 (right). Microbes were colored based on their respective family classification.
1424
1425 **Figure 4. Phylogenetic tree depicting the evolutionary relationship of all**
1426 **retrieved microbial species and assessment of reactive oxygen species (ROS)**
1427 **sensitivity.** The phylogenetic tree was reconstructed based on partial 16S rRNA and
1428 ITS sequences. Nodes are supported based on 500 bootstraps performed in RAxML.
1429 Two fungal species *Rhizopus arrhizus* and *Mucor kunryamgriensis* from the
1430 Mucoroycota were used as outgroups in the tree. Three doses of hydrogen peroxide

1431 (H_2O_2) were used in solid growth media for assessing the growth sensitivity of 69
1432 endophytic strains retrieved from wheat. The percentage of growth inhibition and
1433 promotion is based on the ratio between colony diameter under H_2O_2 and colony
1434 diameter of colonies growing on control plates. Phenotyping performed at 5 days post
1435 inoculation.
1436
1437 **Figure 5. Phenotyping of 69 strains for growth inhibition, promotion, and**
1438 **stability across five time points and three tested exogenous plant secondary**
1439 **metabolites.** A total of 69 isolates representing 59 species were tested in this study.
1440 The three used plant secondary metabolites are cinnamyl alcohol (CA), quinic acid
1441 (QA), and nonanoic acid (NA). The five time points are 24, 48, 72, 96 and 168 hours
1442 after inoculation of microtiter plates. In the alluvial plot, the three strata represent each
1443 phenotype per plant metabolites within a time point, and the connections illustrate the
1444 phenotype of a given microbe between strata. Phenotypes were defined by dividing
1445 the OD of a given strain growing under a plant metabolite by its OD when growing in
1446 the control media. An OD ratio $\geq$ 1.1 indicates growth promotion, $\leq$ 0.9 growth inhibition
1447 and in between stable growth.
1448
1449 **Supplemental Material**
1450
1451 **Figure S1. Validation of apoplastic fluids to isolate proteins and microbes**
1452 **associated with the apoplast compartment of wheat plants.** (A) Scheme showing
1453 the methodology used for isolation of apoplastic fluids from mock-treated and infected
1454 Obelisk and Chinese Spring plants. Apoplastic fluids were then used for microbial
1455 isolation and proteomic analysis. (B) A total of 2’455 proteins were identified in the

1456 wheat apoplastic fluids. Bar plots illustrate the total proteins isolated from the three
1457 biological and two technical replicated for each wheat genotype and treatment. Dark
1458 and light orange bars indicate proteins isolated from mock-treated and infected
1459 Obelisk plants, respectively. Dark and light green bars indicate the proteins isolated
1460 from mock-treated and infected Chinese Spring plants, respectively. (C) A total of 667
1461 microbes were isolated from the apoplastic fluids. Bar plots illustrate the microbes
1462 isolated from each wheat genotype and treatment. Dark and light orange bars indicate
1463 microbes isolated from mock-treated and infected Obelisk plants, respectively. Dark
1464 and light green bars indicate the proteins isolated from mock-treated and infected
1465 Chinese Spring plants, respectively. (D) Western blot analysis for the abundance of
1466 the Rubisco large subunit was used as a marker for intra-cellular contamination of the
1467 apoplastic fluid samples. Histone H3 protein as a general eukaryote positive marker.
1468 (E) Colony morphologies grown on Petri dishes exemplify the microbial diversity
1469 recovered from the apoplastic fluids of each wheat genotype and treatment.
1470
1471 **Figure S2. Contrasting susceptibility or resistance of wheat against**
1472 ***Zymoseptoria tritici* is due to the resistant gene Stb6 and the effector protein**
1473 **AvrStb6.** Representative asymptomatic leaves at 8 days post-inoculation (dpi) show
1474 the biotrophic phase of *Z. tritici* in both the susceptible Obelisk (without the resistant
1475 gene *Stb6*) and the resistant Chinese Spring (with the resistant gene *Stb6*) wheat
1476 plants. Representative leaves at 14 dpi show typical symptoms of *Z. tritici* infection in
1477 the susceptible Obelisk, including the chlorosis, necrosis, and the onset of asexual
1478 reproduction demonstrating by the pycnidial formation. On the other hand, Chinese
1479 Spring plants display a resistant phenotype due to Stb6-AvrStb6 interaction in this
1480 wheat genotype.

1481

1482 **Figure S3. Composition of the wheat-enriched endophytic community-based**
1483 **culture.** Wheat-enriched endophytic community-based culture collection is composed
1484 of 188 purified isolates which were classified taxonomically using partial 16S rRNA
1485 and ITS sequences. (A-C) Bar charts show the phyla-, classes- and families-level
1486 profiles obtained for the microbial diversity recovered from the apoplastic fluids of
1487 mock-treated and infected Obelisk and Chinese Spring wheat genotypes. (D-F) Venn
1488 diagrams showing the number of shared OTUs between groups and for the different
1489 taxonomical classifications (phylum, class, and family). Dashed black circles indicated
1490 the OTU commonly found among the treatments. (D) Proteobacteria and
1491 Actinobacteria were the commonly identified phyla. (E) Actinomycetia,
1492 Alphaproteobacteria and Gammaproteobacteria were the commonly identified
1493 classes. (F) Microbacteriaceae and Psedomonadaceae were the commonly identified
1494 families.

1495

1496 **Figure S4. Overview of antagonistic effect of the wheat-associated microbes**
1497 **against the Dutch IPO323 *Zymoseptoria tritici* isolate.** Species names are
1498 displayed in the bottom right corner (read from left to right). Microbes that did not grow
1499 are listed but were excluded from the data analysis. Three independent Petri dishes
1500 were performed per microbial endophyte.

1501

1502 **Figure S5. Overview of antagonistic effect of the wheat-associated microbes**
1503 **against the Danish Zt05 *Zymoseptoria tritici* isolate.** Species names are displayed
1504 in the bottom right corner (read from left to right). Microbes that did not grow are listed

1505 but were excluded from the data analysis. Three independent Petri dishes were
1506 performed per microbial endophyte.
1507
1508 **Figure S6. Overview of antagonistic effect of the wheat-associated microbes**
1509 **against the Iranian Zt10 *Zymoseptoria tritici* isolate.** Species names are displayed
1510 in the bottom right corner (read from left to right). Microbes that did not grow are listed
1511 but were excluded from the data analysis. Three independent Petri dishes were
1512 performed per microbial endophyte.
1513
1514 **Figure S7. Overview on the antagonistic activity of microbial organisms against**
1515 **three *Zymoseptoria tritici* strains and inhibition phenotypes.** (A) Venn diagram
1516 comparing the count of antagonistic microbes against the three different *Z. tritici*
1517 isolates in the confrontation assays. Each color refers to a different Z. tritici isolate,
1518 such as the Dutch IPO323, the Daish Zt05, and the Iranian Zt10. (B) Portions of gram-
1519 negative or -positive bacteria that inhibited *Z. tritici* isolates in the confrontation assays.
1520 Fisher's exact tests were used to examine the association between the percentage of
1521 isolates inhibiting the *Z. tritici* isolate and the gram stain of the bacteria. (C) The
1522 phylogenetic tree was reconstructed based on partial 16S rRNA and ITS sequences.
1523 Nodes are supported based on 500 bootstraps performed in RAxML. Two fungal
1524 species *Rhizopus arrhizus* and *Mucor kunryamgriensis* from the Mucoroycota were
1525 used as outgroups in the tree. Antagonistic microbes and their interaction with the
1526 three tested *Z. tritici* isolates. The size of the circles is proportionate to the size of the
1527 inhibition zones. Values in the circle correspond to the average size in cm^2 of the three
1528 technical replicates. Red circles represent the antagonistic microbes; white circles

1529 indicate the microbes that did not inhibit *Z. tritici*, and black circles demonstrated the
1530 microbes not tested in these antagonistic assays.
1531
1532 **Table S1.** Overview of the proteomics data of mock-treated and infected Obelisk and
1533 Chinese Spring wheat genotypes with *Zymoseptoria tritici* IPO323 strain.
1534
1535 **Table S2.** The differentially expressed proteins in the Obelisk and Chinese Spring
1536 wheat genotypes at 8 days-post incubation.
1537
1538 **Table S3.** The common 24 overexpressed during *Zymoseptoria tritici* IPO323 strain
1539 infection in Obelisk and Chinese Spring wheat genotypes.
1540
1541 **Table S4.** The most abundant Gene ontology (GO) enrichment terms for the
1542 upregulated proteins (mock vs infected) in Obelisk and Chinese Spring wheat
1543 genotypes.
1544
1545 **Table S5.** The most abundant Gene ontology (GO) enrichment terms for the
1546 downregulated proteins (mock vs infected) in Obelisk and Chinese Spring wheat
1547 genotypes.
1548
1549 **Table S6.** Proteomic analysis identified two up-regulated proteins and one down-
1550 regulated protein from Zymoseptoria tritici during plant-pathogen interaction.
1551
1552 **Table S7.** 188 microbes represent the wheat-enriched endophytic community-based
1553 culture collection used in this study.

1554

1555 **Table S8.** Frequency of each phenotype within five time points and total phenotype

1556 frequency from the microtiter plate experiment.

1557

1558 **Table S9.** Overview on select top 10 bacterial strains with the highest and the lowest

1559 OD ratio per plant compound within each time point.

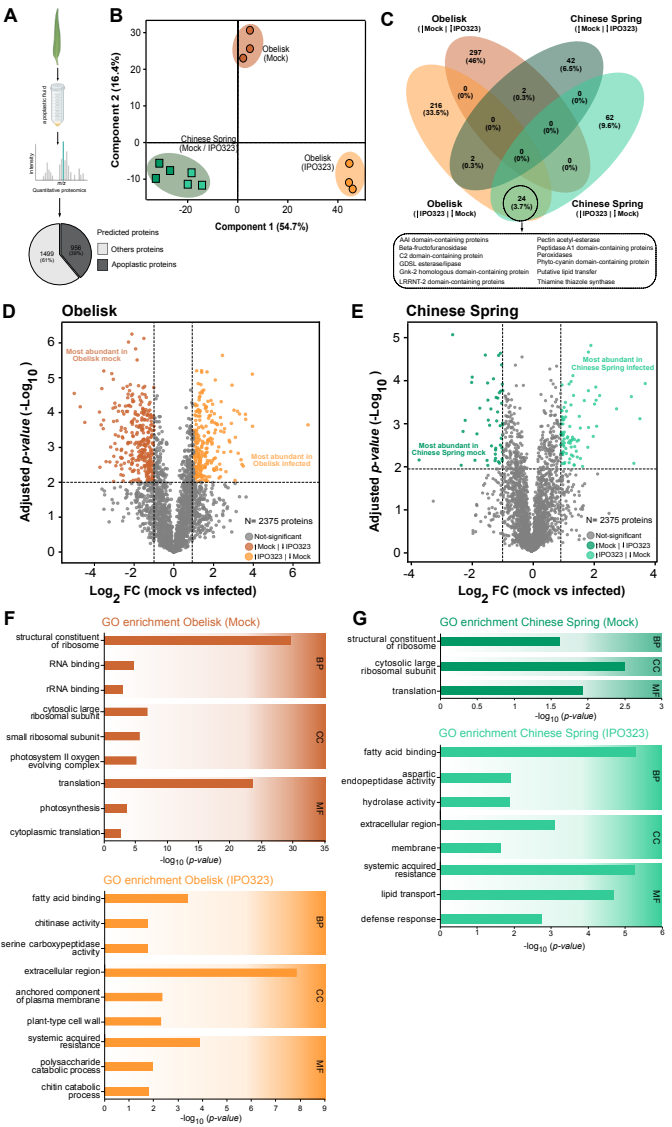
A
apoplastic fluid
intensity
m/z
Quantitative proteomics
1409 (61%)
958 (39%)
Predicted proteins
Others proteins
Apoplastic proteins
B
Obelisk (Mock)
Chinese Spring (Mock / IPO323)
Obelisk (IPO323)
Component 2 (16.4%)
Component 1 (54.7%)
C
Obelisk (Mock | IPO323)
Chinese Spring (Mock | IPO323)
Obelisk (IPO323 | Mock)
Chinese Spring (IPO323 | Mock)
297 (46%)
42 (6.5%)
216 (33.5%)
62 (9.6%)
24 (3.7%)
AAI domain-containing proteins
Beta-fructofuranosidase
C2 domain-containing protein
GDSL esterase/lipase
Gnk-2 homologous domain-containing protein
LRRNT-2 domain-containing proteins
Pectin acetyl-esterase
Peptidase A1 domain-containing protein
Peroxidases
Phytо-cyanin domain-containing protein
Putative lipid transfer
Thiamine thiazole synthase
D
Obelisk
Most abundant in Obelisk mock
Most abundant in Obelisk infected
N= 2375 proteins
Not-significant
Mock | IPO323
IPO323 | Mock
Adjusted p-value (-Log10)
Log2 FC (mock vs infected)
E
Chinese Spring
Most abundant in Chinese Spring infected
Most abundant in Chinese Spring mock
N= 2375 proteins
Not-significant
Mock | IPO323
IPO323 | Mock
Adjusted p-value (-Log10)
Log2 FC (mock vs infected)
F
GO enrichment Obelisk (Mock)
structural constituent of ribosome
RNA binding
rRNA binding
cytosolic large ribosomal subunit
small ribosomal subunit
photosystem II oxygen evolving complex
translation
photosynthesis
cytoplasmic translation
BP
CC
MF
-log10 (p-value)
GO enrichment Obelisk (IPO323)
fatty acid binding
chitinase activity
serine carboxypeptidase activity
extracellular region
anchored component of plasma membrane
plant-type cell wall
systemic acquired resistance
polysaccharide catabolic process
chitin catabolic process
BP
CC
MF
-log10 (p-value)
G
GO enrichment Chinese Spring (Mock)
structural constituent of ribosome
cytosolic large ribosomal subunit
translation
BP
CC
MF
-log10 (p-value)
GO enrichment Chinese Spring (IPO323)
fatty acid binding
aspartic endopeptidase activity
hydrolase activity
extracellular region
membrane
systemic acquired resistance
lipid transport
defense response
BP
CC
MF
-log10 (p-value)

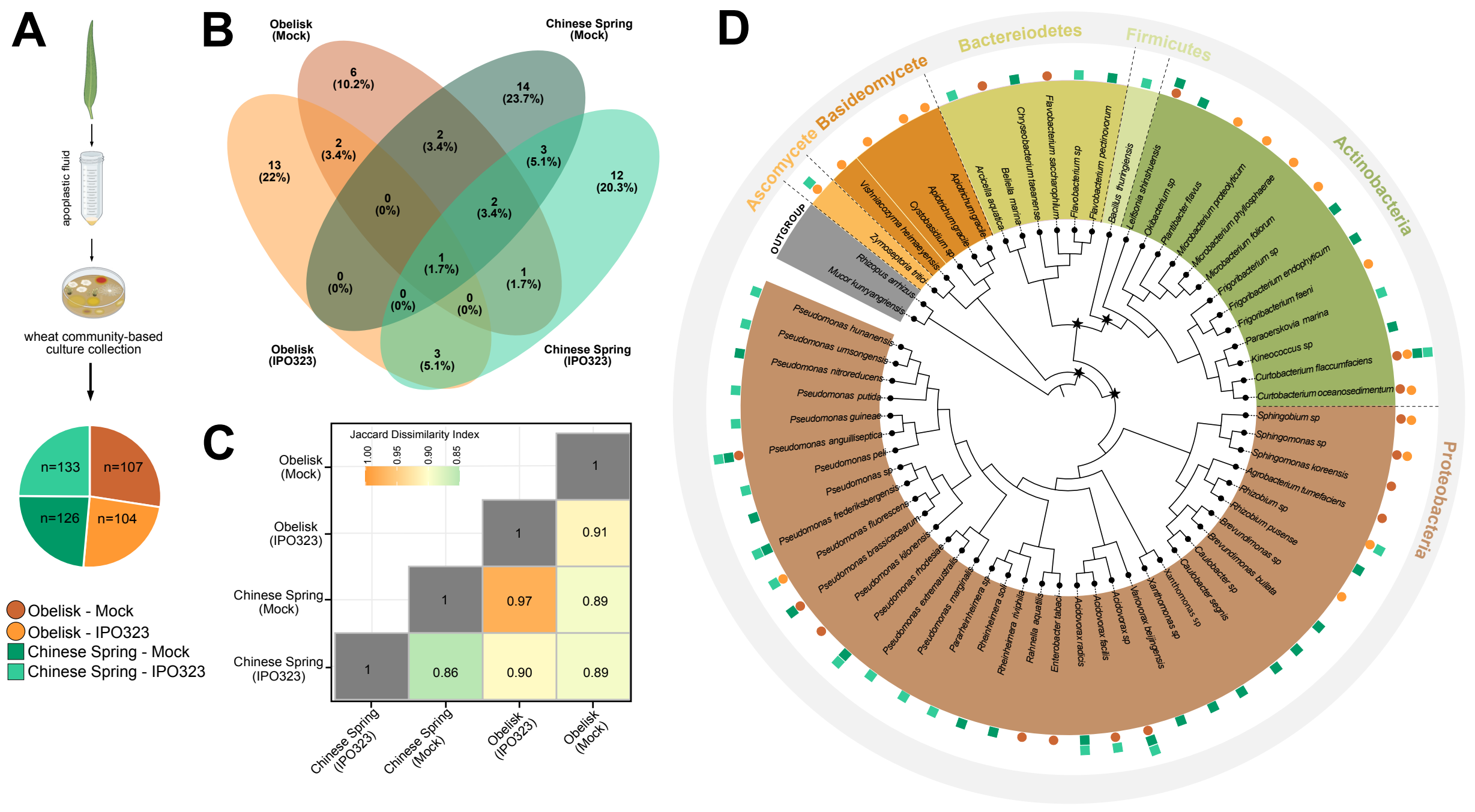
A
apoplastic fluid
wheat community-based culture collection
n=133
n=107
n=126
n=104
Obelisk - Mock
Obelisk - IPO323
Chinese Spring - Mock
Chinese Spring - IPO323
B
Obelisk (Mock)
Chinese Spring (Mock)
Obelisk (IPO323)
Chinese Spring (IPO323)
6 (10.2%)
14 (23.7%)
13 (22%)
12 (20.3%)
2 (3.4%)
2 (3.4%)
3 (5.1%)
0 (0%)
2 (3.4%)
1 (1.7%)
1 (1.7%)
0 (0%)
0 (0%)
0 (0%)
3 (5.1%)
C
Jaccard Dissimilarity Index
1.00
0.95
0.90
0.85
Obelisk (Mock)
Obelisk (IPO323)
Chinese Spring (Mock)
Chinese Spring (IPO323)
1
1
0.91
1
0.97
0.89
1
0.86
0.90
0.89
D
Ascomycete
Basideomycete
Bactereiodetes
Firmicutes
Actinobacteria
Proteobacteria
OUTGROUP
Vishniacozyma heimaeyensis
Zymoseptoria tritici
Cystobasidium sp
Apotrichum gracile
Apiotrichum gracile
Arcicella aquatica
Bellella marina
Chryseobacterium taeanense
Flavobacterium saccharophilum
Flavobacterium sp
Flavobacterium pectinovorum
Bacillus thuringiensis
Leifsonia shinshuensis
Okibacterium sp
Plantibacter flavus
Microbacterium proteolyticum
Microbacterium phyllosphaerae
Microbacterium foliorum
Frigoribacterium sp
Frigoribacterium endophyticum
Frigoribacterium faeni
Paraoerskovia marina
Kineococcus sp
Curtobacterium flaccumfaciens
Curtobacterium oceanosedimentum
Sphingobium sp
Sphingomonas sp
Sphingomonas koreensis
Agrobacterium tumefaciens
Rhizobium sp
Rhizobium pusense
Brevundimonas sp
Brevundimonas bullata
Caulobacter sp
Caulobacter segnis
Xanthomonas sp
Xanthomonas sp
Variovorax beijingensis
Acidovorax sp
Acidovorax facilis
Acidovorax radicis
Enterobacter tabaci
Rahnella aquatilis
Rheinheimera nivipthia
Rheinheimera sp
Pararheinheimera sp
Pseudomonas marginalis
Pseudomonas extremaustralis
Pseudomonas rhodesiae
Pseudomonas kilonensis
Pseudomonas brassicacearum
Pseudomonas fluorescens
Pseudomonas frederiksbergensis
Pseudomonas sp
Pseudomonas peli
Pseudomonas anguilliseptica
Pseudomonas guineae
Pseudomonas putida
Pseudomonas nitroreducens
Pseudomonas umsongensis
Pseudomonas hunanensis
Rhizopus arrhizus
Mucor kunyangriensis

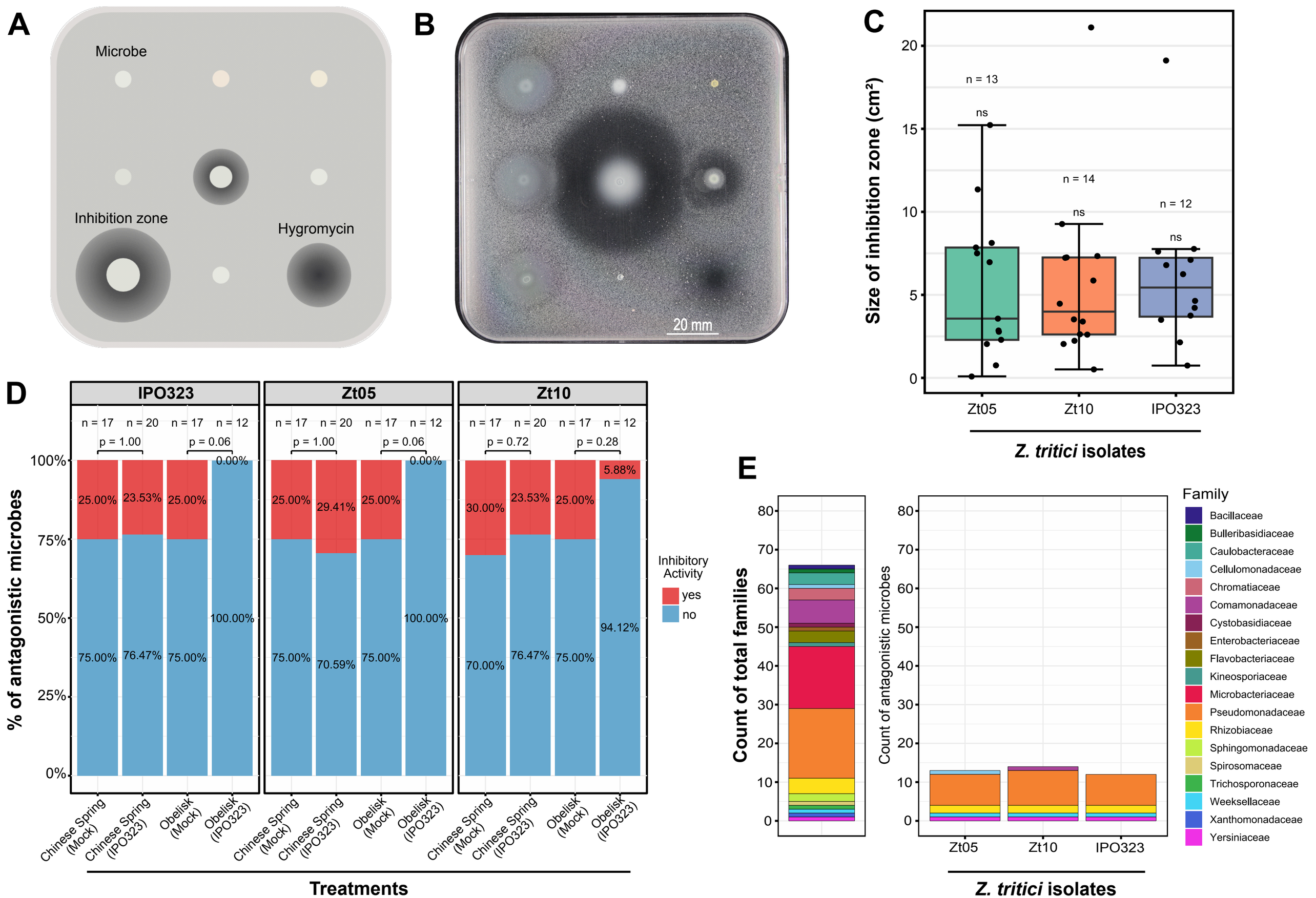
A
Microbe
Inhibition zone
Hygromycin
B
20 mm
C
Size of inhibition zone (cm²)
n = 13
ns
n = 14
ns
n = 12
ns
Zt05
Zt10
IPO323
Z. tritici isolates
D
IPO323
Zt05
Zt10
% of antagonistic microbes
p = 1.00
p = 0.06
p = 0.72
p = 0.28
25.00%
23.53%
0.00%
75.00%
76.47%
100.00%
29.41%
70.59%
30.00%
5.88%
94.12%
Inhibitory Activity
yes
no
Chinese Spring (Mock)
Chinese Spring (IPO323)
Obelisk (Mock)
Obelisk (IPO323)
Treatments
E
Count of total families
Count of antagonistic microbes
Family
Bacillaceae
Bulleribasidiaceae
Caulobacteraceae
Cellulomonadaceae
Chromatiaceae
Comamonadaceae
Cystobasidiaceae
Enterobacteriaceae
Flavobacteriaceae
Kineosporiaceae
Microbacteriaceae
Pseudomonadaceae
Rhizobiaceae
Sphingomonadaceae
Spirosomaceae
Trichosporonaceae
Weeksellaceae
Xanthomonadaceae
Yersiniaceae
Zt05
Zt10
IPO323
Z. tritici isolates

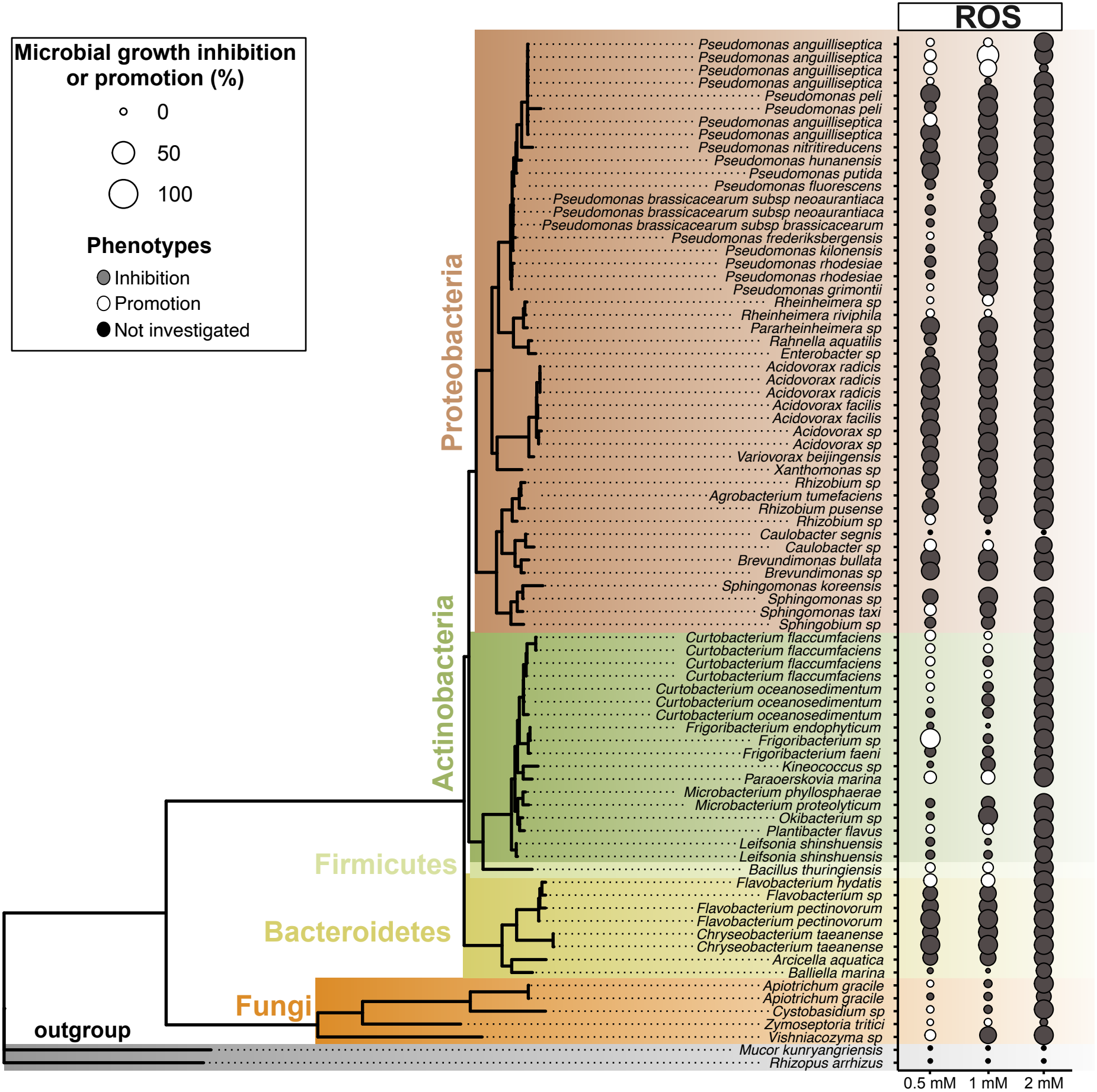
Microbial growth inhibition or promotion (%)
0
50
100
Phenotypes
Inhibition
Promotion
Not investigated
ROS
Proteobacteria
Actinobacteria
Firmicutes
Bacteroidetes
Fungi
outgroup
Pseudomonas anguilliseptica
Pseudomonas anguilliseptica
Pseudomonas anguilliseptica
Pseudomonas anguilliseptica
Pseudomonas peli
Pseudomonas peli
Pseudomonas anguilliseptica
Pseudomonas anguilliseptica
Pseudomonas nitritireducens
Pseudomonas hunanensis
Pseudomonas putida
Pseudomonas fluorescens
Pseudomonas brassicacearum subsp neoaurantiaca
Pseudomonas brassicacearum subsp neoaurantiaca
Pseudomonas brassicacearum subsp brassicacearum
Pseudomonas frederiksbergensis
Pseudomonas kilonensis
Pseudomonas rhodesiae
Pseudomonas rhodesiae
Pseudomonas grimontii
Rheinheimera sp
Rheinheimera riviphila
Pararheinheimera sp
Rahnella aquatilis
Enterobacter sp
Acidovorax radicis
Acidovorax radicis
Acidovorax radicis
Acidovorax facilis
Acidovorax facilis
Acidovorax sp
Acidovorax sp
Variovorax beijingensis
Xanthomonas sp
Rhizobium sp
Agrobacterium tumefaciens
Rhizobium pusense
Rhizobium sp
Caulobacter segnis
Caulobacter sp
Brevundimonas bullata
Brevundimonas sp
Sphingomonas koreensis
Sphingomonas sp
Sphingomonas taxi
Sphingobium sp
Curtobacterium flaccumfaciens
Curtobacterium flaccumfaciens
Curtobacterium flaccumfaciens
Curtobacterium flaccumfaciens
Curtobacterium oceanosedimentum
Curtobacterium oceanosedimentum
Curtobacterium oceanosedimentum
Frigoribacterium endophyticum
Frigoribacterium sp
Frigoribacterium faeni
Kineococcus sp
Paraoerskovia marina
Microbacterium phyllosphaerae
Microbacterium proteolyticum
Okibacterium sp
Plantibacter flavus
Leifsonia shinshuensis
Leifsonia shinshuensis
Bacillus thuringiensis
Flavobacterium hydatis
Flavobacterium sp
Flavobacterium pectinovorum
Flavobacterium pectinovorum
Chryseobacterium taeanense
Chryseobacterium taeanense
Arcicella aquatica
Balliella marina
Apiotrichum gracile
Apiotrichum gracile
Cystobasidium sp
Zymoseptoria tritici
Vishniacozyma sp
Mucor kunryangriensis
Rhizopus arrhizus
0.5 mM
1 mM
2 mM

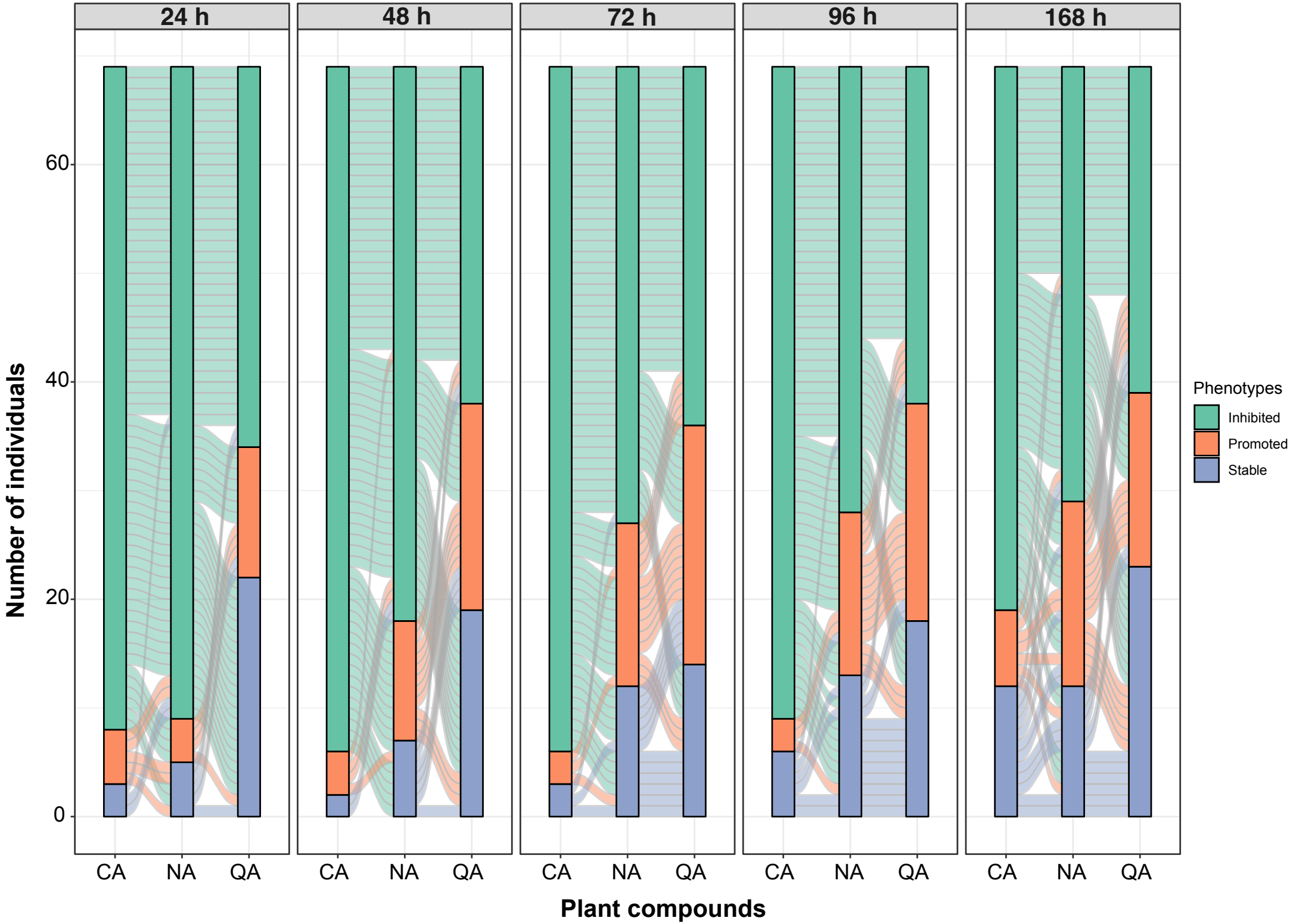
24 h
48 h
72 h
96 h
168 h
Number of individuals
0
20
40
60
CA
NA
QA
Plant compounds
Phenotypes
Inhibited
Promoted
Stable